Possible Protective Effects of Quercetin versus Quercetin Loaded Chitosan Nanoparticles on Zinc Sulfate Induced Olfactory Mucosa and bulb Injury in Adult Male Albino Rats; Behavioral, Biochemical, Histological and immunohistochemical study

Original Article

Aliaa Hamdy AbdelHaleem[1], Amira Fathy Ahmed[1], Randa Ahmed Ibrahim[1], Sayed Fouad EL Sheikh[2], Walaa Yehia Abdelzaher[3], Azza` Hussien Ali[1], Sara Mohamed Naguib Abdel Hafez[1]

[1]Department of Histology and Cell Biology, [2]Department of Anatomy and Embryology, [3]Department of Medical Pharmacology, Faculty of Medicine, Minia University, Minia, Egypt

ABSTRACT

Background: Anosmia is a common annoying problem that affects quality of life. Nanoparticles act as nanocarriers that deliver potent drug payloads at a controlled rate at the target site.

Purpose: This current work aimed to evaluate the potential preventive benefits of Quercetin (QU) versus Quercetin-loaded chitosan nanoparticles (QU-CSNPs) on an experimental rat model of anosmia and shed insight on its protective mechanisms.

Methods: Forty rats were randomly divided into four groups, the Control group, the Zinc sulfate (ZnS) group, the ZnS+QU group, and the ZnS+QU-CSNPs group. Behavioral assessment was carried out. Olfactory mucosae and bulbs were collected for biochemical, histological, immunohistochemical, and morphometric analysis.

Results: The ZnS group showed behavioral alternation, decreased glutathione levels, increased malonaldehyde, and tumor necrosis factor-α levels. Olfactory mucosa and bulb showed histological alterations, as well as a significant increase in COX-2 immune-expression and decrease in PCNA and SOX2 expression. The ZnS+QU-CSNPs group showed amelioration in previously mentioned parameters and histological alternation than the ZnS+QU group.

Conclusions: QU-CSNPs has prophylactic effects in an anosmia model than QU via its anti-inflammatory and antioxidant effects. This could pave the way for additional studies to investigate further mechanisms underlying the potential beneficial effects of QU-CSNPs and bring up a new line for anosmia therapy.

Key Words: Olfactory Mucosa, quercetin, quercetin Loaded Chitosan Nanoparticles, zinc sulfate.

Revised: 13 June 2024, **Accepted:** 03 July 2024

Corresponding Author: *Aliaa Hamdy AbdelHaleem*, *Department of Histology and Cell Biology, Faculty of Medicine, Minia University, Minia, Egypt,* **Tel.:** *+201121825339*, **E-mail:** *faahata87@gmail.com.*

ISSN: 1110-0559, December 2023, Vol. 7, No. 2.

INTRODUCTION

Anosmia is characterized by a diminished or absent sense of smell[1]. The prevalence of anomia is high and it significantly affects mortality and quality of life. Those who suffer from anosmia may find it difficult to enjoy their meals since they lack a sense of taste. The outcome can be a loss of weight or malnutrition. Unfortunately, depression is a possible side effect of anosmia, which makes it hard to appreciate pleasant flavors or odors[2]. People who have a lack of smell often experience heightened worry when it comes to potentially dangerous items, such as gas or spoiled food[3]. As a common symptom of coronavirus disease 2019 (COVID-19), anosmia, or loss of smell, has garnered more attention during the severe acute respiratory syndrome coronavirus2 (SARS-CoV-2)[4].

There are three distinct forms of olfactory dysfunctions. The first category is conductive diseases caused by obstruction of the nasal canals and hence impairment of odorant transmission to the olfactory epithelium. The 2nd type is damage to the olfactory nerve, leading to sensorineural loss. The 3rd type is damage to the central nervous system's olfactory processing pathway leading to central malfunction[5].

Zinc sulfate (ZnS), is frequently used in zinc dietary supplements[6]. The ZnS is an ingredient in over-the-counter rhinovirus treatments in the form of nasal swabs and sprays[7]. Intranasal perfusion of ZnS disrupts the main olfactory epithelium, a crucial component of olfactory perception. Several studies demonstrated that direct application of a ZnS solution to the olfactory mucous membrane of rats, pigeons,

 DOI: 10.21608/jmh.2024.297558.1130

mice and hamsters inhibits olfactory function[8]. Additionally COVID-19-related anosmia may arise from a temporary loss of function of supporting cells in the olfactory epithelium, which indirectly leads to disturbed olfactory sensory neurons[9].

Quercetin (QU) is a naturally found flavonoid present in many fruits, vegetables and nuts and is recognized to have many health benefits[10]. Quercetin has been extensively studied for its anti-inflammatory, antioxidant, antibacterial, anti-Alzheimer's, antiarthritic, cardiovascular, wound-healing and anticancer properties, thus, people may experience its protective effects just by incorporating it into their diets or taking it as a dietary supplement[11]. Despite having a wide range of pharmacological actions, in vivo use of QU is constrained by its low water solubility, poor bioavailability, oxidant instability and extreme biotransformation limitation[12]. Quercetin in its nano formulations is used to tackle these issues. Hydrophobic medications like QU delivered by nanoparticles have significant benefits such as high encapsulation efficiency, prolonged circulation time, controlled release and improved therapeutic efficacy[13]. Quercetin is a well-known antioxidant with anti-inflammatory, anti-SARS-CoV-2 and immunomodulatory properties. As a result, it is thought that quercetin has every quality needed for COVID-19 treatment[14].

Nanoparticles (NPs) act as nanocarriers, delivering strong pharmacological payloads at a controlled rate at the targeted site. Due to their small size (1 – 100 nm), nanoparticles can more readily pass through blood capillaries without being removed by phagocytic cells, allowing for longer drug administration and an extension of their plasma half-life[15].

Chitosan, a natural polymer, can be found in the cell walls of crustaceans, fungus, insects, algae, microbes and some invertebrate animals[16]. It is often used to make drug delivery nano systems that allow targeted treatment without toxicity because of its unique features, such as being biocompatible, biodegradable and having mucoadhesive capabilities[17].

This current work aimed to evaluate the potential preventive benefits of Quercetin (QU) versus Quercetin-loaded chitosan nanoparticles (QU-CSNPs) on an experimental rat model of anosmia and shed insight on its protective mechanisms.

MATERIALS AND METHODS

Animals:

This study was carried out in the Histology and Cell Biology Department, Faculty of Medicine, Minia University in Egypt. All animal procedures were carried out in accordance with the local guidelines established by the Faculty of Medicine's ethics committees (permission No. 95:2021). The animal experiment adhered to the ARRIVE (Animal Research: Reporting of In Vivo studies) principles and was conducted in compliance with the UK Animals (Scientific Procedures) Act of 1986 and its related guidelines, as well as EU Directive 2010 / 63 / EU for animal research. The animals utilized in this study were purchased from Minia University's Faculty of Agriculture growing center. The study included 40 mature male albino rats (Sprague Dawley) that appeared to be pathologically free. Rats were 8 - 10 weeks old and weighed between 150 - 200 grams. All the rats seemed to be pathogen-free. Rats were housed in clean plastic cages, fed a standard laboratory diet and given unlimited access to water and food. They were kept in a clean, well-ventilated room. Rats were housed at a laboratory temperature of 24 - 30ºC and on a 12-hour light/12-hour darkness cycle.

Preparation of quercetin loaded Chitosan nanoparticles (Q-CSNPs):

According to manufacturer’s instructions (Nano Gate Egypt) material data sheet, Web site: www.nanogate-eg.com).

Preparation of Chitosan nanoparticles:

The ionotropic gelation technique was used to prepare chitosan nanoparticles (NPs). An aqueous solution of tripolyphosphate (TPP) (Merck Millipore, Germany catalog No.1069991000) was added to a solution of chitosan to produce blank nanoparticles. In brief, 1 gm of Chitosan powder (Loba Chemie, India catalog No. 02697) was dissolved in 200 ml 1 % glacial acetic acid (Loba Chemie, India catalog No. 3051D) (pH = 4) and shaken for 6 h to create homogenous solution then, 150 ml of TPP 0.2 % w/v was added dropwise. After then, the clear solution turned turbid, suggesting the formation of CSNPs. The suspension was then centrifuged three times for 30 minutes at 9000 rpm using DH2O[18].

Preparation of quercetin Encapsulated CSNPs:

Qu-loaded TPP-Chitosan NPs were formed by adding 1 ml of Qu ethanol solution at a concentration of 3 mg/ml to CS solution dropwise before adding TPP. The NPs underwent the above-mentioned cleaning.

Tests: Size and shape: TEM (Transmission Electron Microscope) were done using a JEOL JEM-2100 high resolution transmission electron microscope with an accelerating voltage of 200 kV (Figure 1a).

Induction of anosmia:

Using a 1-ml syringe connected to an inserted polypropylene tube (Size PE 20, Shanghai Jingyu Plastic Products Co., Ltd., China), a 0.2 ml volume of either saline solution (Sodium chloride solution Sigma-Aldrich Chemie GmbH, Germany, catalog No S8776) and 10 % zinc sulfate solution (isotonic) (Zinc sulphate heptahydrate, (ZnSo4.7H2O,), PIOCEM for laboratory chemicals, Egypt. Catalog No. Z004) was gradually administered by the syringe. The tube extended 12 cm from the syringe, but only 2 cm of its tip was inserted into the nose. Rotating the tube with the thumb and index finger made it easier to insert to a premarket indicator point on the tube, which was printed with permanent ink. After the intranasal irrigation was finished and the tube was removed, the animal was held down and the nose tip was gently pressed against an absorbent cloth until it recovered from the ether. The intranasal irrigation of zinc sulfate was repeated every 5 days over a 2-week test period to provide sustained anosmia[19, 20].

Rats' olfactory ability was assessed using the buried food test[21]. The testing food should be particularly tasty to the animals. The experiment's technique spans 3 consecutive days. 1st day, the animals were placed in clean cages with a 3-cm layer of fresh cage bedding. Ordinary food was replaced with the testing cookies. The next morning, the cages were inspected to ensure that the cookies had been consumed. The 2nd day, food was hidden, leaving the rat to fast overnight. After 17 hours of fasting, rats were placed separately in a clean cage with fresh bedding on 3rd day and allowed to acclimatize for 5 minutes before testing. A piece of cookie was hidden in a random corner and the rat was returned to the cage. The rat's time taken to collect the biscuit with its forepaws was timed within a 15-minute constraint. The test was conducted first to exclude anosmic rats from the experiment and then was repeated on days 9, 14, 20 and 21 to evaluate the effect of ZnS, QU and QU-CSNPs on olfaction.

Experimental design:

The total period of the study was three weeks. Forty adult male albino rats were randomly divided into four equal groups, ten rats for each group (Figure 1b). Group I (Control group); Rats were subdivided into two groups; group Ia, received intranasal irrigation of 0.2 ml saline solution every 5 days starting from the 8th day. Group Ib, rats received intravenous injection of 0.5 ml PEG 400 which acts as a solvent of quercetin (1:1dilution with distilled water) via tail vein twice a week through the whole experiment period. Group II (ZnS- group); rats were irrigated intranasally with 0.2 ml volume of 10 % Zinc sulfate solution every 5 days starting from the 8th day till the end of the experiment. Group III (ZnS+ QU- group); Rats received intravenous injection of 25 mg /kg Quercetin dissolved in 50 % PEG 400 (Loba chemie, India. catalog No.00259) [22] via tail vein twice a week from the beginning of the experiment one week before induction of anosmia and continued through the experiment along with zinc sulfate nasal irrigation. Group IV (ZnS+ QU-CSNPs group); Rats received intravenous injection of 25 mg /kg Quercetin loaded chitosan nanoparticles[22] via tail vein twice a week from the beginning of the experiment one week before induction of anosmia and continued through the experiment along with zinc sulfate nasal irrigation.

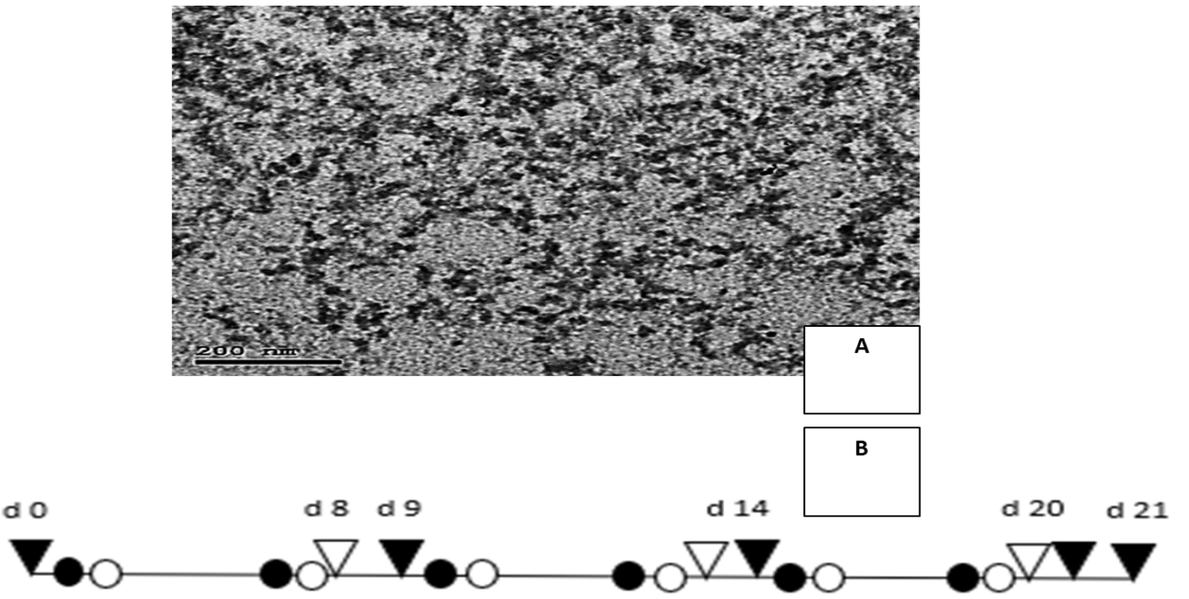

Figure 1a: Showing: A) TEM image of QU-CSNPs (Nano Gate material data sheet). B) Time course of the experimental design. ▼; Behavior test, ∇; A time point of intranasal irrigation of zinc sulfate, ●; A time point of Quercetin loaded chitosan nanoparticles treatment, O; A time point of Quercetin treatment.

At the end of the experiment, all rats from all groups were sacrificed under light halothane anesthesia. Excess skin, muscle and other soft tissues were removed from the heads, the lower jaws were removed. The skulls were opened and complete brains were dissected out. Some specimens of heads and brains were rapidly fixed in 10 % formal saline for light microscopic processing and others were fixed in glutaraldehyde for electron microscopic processing and others were processed for biochemical study.

Biochemical study:

Using scissors, the lower jaw was removed to liberate the nasal septum for the olfactory mucosa. After that, a rongeur assisted in the elimination of the facial muscles on both sides. A rongeur was used to remove the nasal cavity's covering one side at a time, beginning at the back of the incisors. The olfactory turbinates were carefully removed with forceps once they were visible as orange or brown organs in the rear of the nose. The olfactory mucosa was isolated by cutting the tissue along the arc of the perpendicular plate, the cribriform plate and the nasal cavity ceiling using a 26 gauge needle[23].

The rats' brain tissues were removed from their skulls and the olfactory bulbs were subsequently dissected for the specimens[24, 25].

Olfactory mucosa and bulb samples were homogenized in potassium phosphate buffer (10 mM, pH 7.4). The ratio of tissue weight to homogenization buffer was 1:10. The homogenates were centrifuged at 4000 g for 10 minutes at 4°C. The resultant supernatant was used to evaluate malondialdehyde (MDA); MDA level is an indication of lipid peroxidation and was determined using the Buege and Aust technique (1978). Glutathione (GSH) level, antioxidant markers, tumor necrotic factor -α (TNF-α) and inflammation markers were all measured. Both GSH and TNF-α levels were measured using commercial kits. GSH was tested colorimetrically using kits (Code No.GR 25 11) bought from Biodiagnostic in Egypt. TNF-α was tested using ELISA kits (Code No. E-EL-R2856) purchased from Elabscience, USA.

Histological study:

For light microscopic examination:

The head and brain samples were fixed in 10 % neutral-buffered formalin at room temperature for 24 hours. After proper fixation, the head specimens were decalcified for one week in 10 % EDTA - pH 7.3 at 4°C (Bryche *et al.*, 2020). The head and brain samples were then dehydrated in a graded alcohol series, cleaned with xylene and embedded in paraffin wax. After cutting with a microtome,

5µm sections were mounted on glass slides and stained with Hematoxylin and Eosin. Other sections were processed for histochemical demonstration of polysaccharides (acid muco-substances) using Alcian Blue (AB) at pH 2.5 and the Periodic Acid-Schiff (PAS) method for neutral muco-substances[26].

Immunohistochemistry was used on 5µm sections to identify SOX2, PCNA and COX2. Briefly, sections were deparaffinized in xylene, rehydrated in declining alcohol grades and submerged in 0.1 % hydrogen peroxide for 15 minutes to inhibit endogenous peroxidase activity. Then sections washed by phosphate buffer, followed by incubation in the ultra-vision block for 5 minutes at room temperature to block the nonspecific background staining. The primary antibodies used were anti-SOX2 antibody (polyclonal rabbit antibodies, catalog No. PAS-85144) anti-PCNA antibody (polyclonal rabbit antibodies, catalog No. MA5 - 11358) and anti-COX2 antibody (monoclonal mouse antibodies, Catalog No. MA5 - 45052) obtained from Thermo Fisher scientific, USA.

The primary anti-PCNA antibody was ready to be used and incubated with the tissue for 60 minutes at room temperature. The primary anti-COX2 was diluted at 1:100 in antibody diluent and incubated with the tissue for 30 minutes at room temperature. The primary anti-SOX2 was diluted at 1:500 in antibody diluent and incubated with the tissue for 30 minutes at room temperature. Then washed with PBS, incubated with the secondary antibody (Vector laboratory 1:2000). The reaction was observed using the Ultra-Vision One Detection System, HRP Polymer and (diaminobenzidine) DAB Plus Chromogen (Thermo Fisher Scientific, USA). After the reaction was completed, hematoxylin was used to counterstain it and it was dehydrated by passing through escalating alcohol concentrations before being cleaned with xylene. Then a cover slip with permanent mounting material was utilized[27]. Immunoreactivity was detected as dark brown cytoplasmic staining for COX2 and nuclear staining for PCNA and SOX2.

In negative control slides, the same steps were applied but the primary antibodies were not added. The positive control for COX_2 was lung carcinoma, for SOX2 was rat brain stem and for PCNA was of mouse normal testis

For Transmission Electron Microscopic study:

The Assiut University Electron Microscopy Unit prepared the ultrathin sections, while the Central Lab examined the stained sections. The stained sections were examined in Central Lab. For Microanalysis and Nanotechnology, Minia University. Ultra-thin sections for transmission electron microscopy (TEM) were generated using the approach described by Cheville and Stasko (2014). In brief, tiny portions (1 mm) of olfactory bulb and olfactory mucosa (carefully detached from the bone) were immediately preserved in 2.5 % glutaraldehyde in 0.1M cacodylate buffer at pH 7.4 for 24 hours at 4°C. The specimens were then rinsed with the buffer and post-fixed in 1 % osmium tetroxide in distilled water for 2 hours at 4°C. Specimens were dehydrated with increasing concentrations of ethanol and embedded in epoxy resin. Semithin 1µm slices were cut with glass knives using Power Tone XL (USA) and stained with toluidine blue for inspection under light microscopy. Ultrathin sections (7080- nm) were cut with glass blades on a Power Tone XL (USA) ultra-microtome, mounted on grids and stained with uranyl acetate and lead citrate for examination.

Photography:

Light micrographs were captured in the Histology and Cell Biology Department's light microscopic unit at Minia University using a high-resolution color digital camera mounted on a BX51 microscope (Olympus, Japan). The camera was connected to a computer programmed with LC micro application software. Transmission electron microscopy (JEM-100 CX II, Japan) was used to capture ultra-structural images.

Morphometric study:

Morphometric analysis was done in standard high-power field (X400) in 10 non overlapping fields from each rat for each group using Image J (https://rsbweb.nih.gov/ij/; NIH, Bethesda, MD) software to study: a) Olfactory epithelium thickness (µm). b) Mean number of PCNA and SOX2 immunopositive cells. c) Mean area fraction of COX2 immunopositivity. d) Olfactory epithelium thickness.

Statistical analysis:

The quantitative data was analyzed using Graph Pad Prism (version 9.01 for Windows, Graph Pad Software, San Diego, California, USA, www.graphpad.com). Each group's parameters were calculated to determine their mean and standard deviation (SD). Values were reported as mean ± SD. A one-way analysis of variance (ANOVA) test was performed to discover significant differences between groups, followed by the Tukey-Kramer post-hoc test for multiple comparisons. *P*-values < 0.05 indicated statistical significance.

RESULTS

Both subgroups Ia and Ib showed the same behavioral, biochemical, histological and immunohistochemical results thus one representative group was used.

Buried food test results:

The duration of finding food showed a significant increase in ZnS group when compared to the control group ($P < 0.000$). In ZnS+QU treated group, there was a significant increase when compared to control group ($P < 0.000$) and insignificant difference with ZnS group. As regard ZnS+ QU-CSNPs treated group, there was a significant decrease when compared to both ZnS and ZnS+QU treated groups ($P < 0.000$) and a significant increase if compared to control group ($P < 0.000$) (Table1).

Table 1: The mean values of latency to find the cookie in different groups (n = 6):

Group	Day 9		Day 14		Day 20		Day 21	
	Mean ± SD	*P* value	Mean ± SD	*P* value	Mean ± SD	*P* value	Mean ± SD	*P* value
Control group	55.67 ± 11.27		52.83 ± 10.30		54.50 ± 13.84		60.67 ± 19.83	
ZnS group	900 ± 0.000	< 0.000c*	900 ± 0.000	< 0.000c*	900.0 ± 0.000	<0.000c*	900.0 ± 0.000	< 0.000c*
ZnS + QU treated group	859.2. ± 40.05	< 0.000c* 0.058Z	887.5 ± 20.92	< 0.000c* 0.599Z	895.4 ± 10.00	<0.000c* 0.883Z	893.3 ± 12.11	< 0.000c* 0.950Z
ZnS + QU - CSNPs treated group	166..7 ± 31.25	< 0.000C* < 0.000Z* < 0.000Z+Q*	152.3 ± 25.37	< 0.000C* < 0.000Z* < 0.000 Z+Q*	113.5 ± 16.47	< 0.000C* < 0.000Z* < 0.000 Z + Q*	146.7 ± 36.56	< 0.000C* < 0.000Z* < 0.000 Z + Q*

[c] versus the control group, Z versus ZnS group and Z + Q versus the Q - treated group. *$P < 0.05$ is significant.

Biochemical results:

The ZnS group showed a significant increase in olfactory mucosa MDA and olfactory bulb MDA with a significant decrease in mucosa GSH and olfactory bulb GSH when compared to control group. On the other hand, ZnS+QU treated and ZnS+QU-CSNPs treated groups showed a significant decrease in olfactory mucosa MDA and olfactory bulb MDA with a significant increase in mucosa GSH and olfactory bulb GSH when compared to ZnS group. ZnS+QU-CSNPs treated group showed a significant decrease in olfactory mucosa MDA and olfactory bulb MDA with a significant increase in olfactory mucosa GSH and olfactory bulb GSH when compared to both ZnS group and ZnS+QU treated group (Table 2).

Table 2: The mean levels of the olfactory mucosa and olfactory bulb MDA and GSH in different groups (n = 6):

Group	Olfactory mucosa MDA (nmol/g tissue)		Olfactory bulb MDA(nmol/g tissue)		Olfactory mucosa GSH (nmol/g tissue)		Olfactory bulb GSH (nmol/g tissue)	
	Mean ± SD	*P* value	Mean ± SD	*P* value	Mean ± SD	*P* value	Mean ± SD	*P* value
Control group	20.13 ± 4.79		47.70 ± 7.38		62.45 ± 8.38		43.89 ± 7.13	
ZnS group	58.88 ± 6.33	$< 0.000^{c*}$	93.48 ± 5.76	$< 0.000^{c*}$	32.24 ± 4.00	$< 0.000^{c*}$	18.39 ± 5.02	$< 0.000^{c*}$
ZnS +QU treated group	38.25 ± 5.29	$< 0.000^{c*}$ $< 0.000Z^{*}$	66.53 ± 6.54	$< 0.000^{c*}$ $< 0.000Z^{*}$	45.68 ± 7.03	0.000^{c*} $0.003Z^{*}$	32.94 ± 5.15	0.000^{c*} $0.014Z^{*}$
ZnS+ QU-CSNPs treated group	13.80 ± 5.45	0.128^{c} $< 0.000Z^{*}$ 0.001 Z+Q*	49.24 ± 8.64	0.973^{c} $< 0.000Z^{*}$ 0.000 Z+Q*	58.41 ± 8.05	0.667^{c} $< 0.000Z^{*}$ 0.006 Z+Q*	45.33 ± 8.77	0.972^{c} $< 0.000Z^{*}$ 0.004 Z+Q*

[c] versus the control group, Z versus ZnS group and Z+Q versus the Q - treated group.*$P < 0.05$ is significant.

The ZnS group showed a significant increase in olfactory mucosa TNF-α and olfactory bulb TNF-α when compared to other groups. Meanwhile, ZnS+QU treated and ZnS+QU-CSNPs treated groups showed a significant improvement in TNF-α when compared to ZnS nasal irrigation group. ZnS+QU-CSNPs treated group showed a significant decrease in olfactory mucosa TNF-α and olfactory bulb TNF-α when compared to ZnS+QU treated group (Table 3).

Table 3: The mean levels of the olfactory mucosa and olfactory bulb TNF-α in different groups (n = 6):

Group	Olfactory mucosa TNF-α (pg/mg tissue)		Olfactory bulb TNF-α (pg/mg tissue)	
	Mean ± SD	*P* value	Mean ± SD	*P* value
Control group	13.65 ± 3.29		26.44 ± 4.75	
ZnS group	46.37 ± 10.53	$< 0.000^{c*}$	91.02 ± 12.60	$< 0.000^{c*}$
ZnS +QU treated group	29.31 ± 2.66	0.000^{c*} $< 0.000Z^{*}$	46.60 ± 7.09	0.000^{c*} $< 0.000Z^{*}$
ZnS+ QU-CSNPs treated group	19.57 ± 5.56	0.262^{c} $< 0.000Z^{*}$ $0.022\ Z+Q^{*}$	29.60 ± 7.28	0.875^{c} $< 0.000Z^{*}$ $0.002\ Z+Q^{*}$

[c] versus the control group, Z versus ZnS group and Z+Q versus the Q - treated group.*$P < 0.05$ is significant.

Histological results:

Light microscopic results:

Olfactory mucosa Hematoxylin and eosin (H and E) results:

The control olfactory mucosa was formed of a pseudostratified columnar epithelium. This epithelium was formed of supporting cells; had oval pale nuclei arranged in the upper part of the epithelium, while the olfactory receptor cells nuclei were rounded and contained chromatin clumps, which occupy the middle part of the epithelium. The basal cells included horizontal and globose cells, which were situated next to the basement membrane. Their nuclei were elongated with their long axis parallel to the basement membrane The lamina propria contained Bowman's glands, nerve bundles and blood capillaries Figures 2a1 and 2a2. The ZnS group showed areas of damaged and apparently shrunken olfactory mucosa with desquamation of epithelium (Figure 2b1), there was thinning of the olfactory epithelium with loss of its normal histological architecture, basal cells were preserved and the lamina propria showed degenerated nerve bundles, degenerated Bowman's glands with pyknotic nuclei, vacuolated cytoplasm and irregular outlines (Figure 2b2). The ZnS+QU treated group showed replacement of olfactory epithelial cells with columnar ciliated cells and goblet cells. The lamina propria showed dilated Bowman's glands (Figures 2c1 and 2c2). The ZnS+ QU-CSNPs treated group showed apparently preserved architecture of olfactory mucosa. The olfactory epithelium appeared with its cell types: supporting cells in the upper part of the epithelium, olfactory neurons in the middle part and basal cells next to the basement membrane. Ducts of Bowman's glands among epithelium were apparent. The lamina propria showed nerve bundles, dilated Bowman's glands and dilated blood capillaries (Figures 2d1 and 2d2).

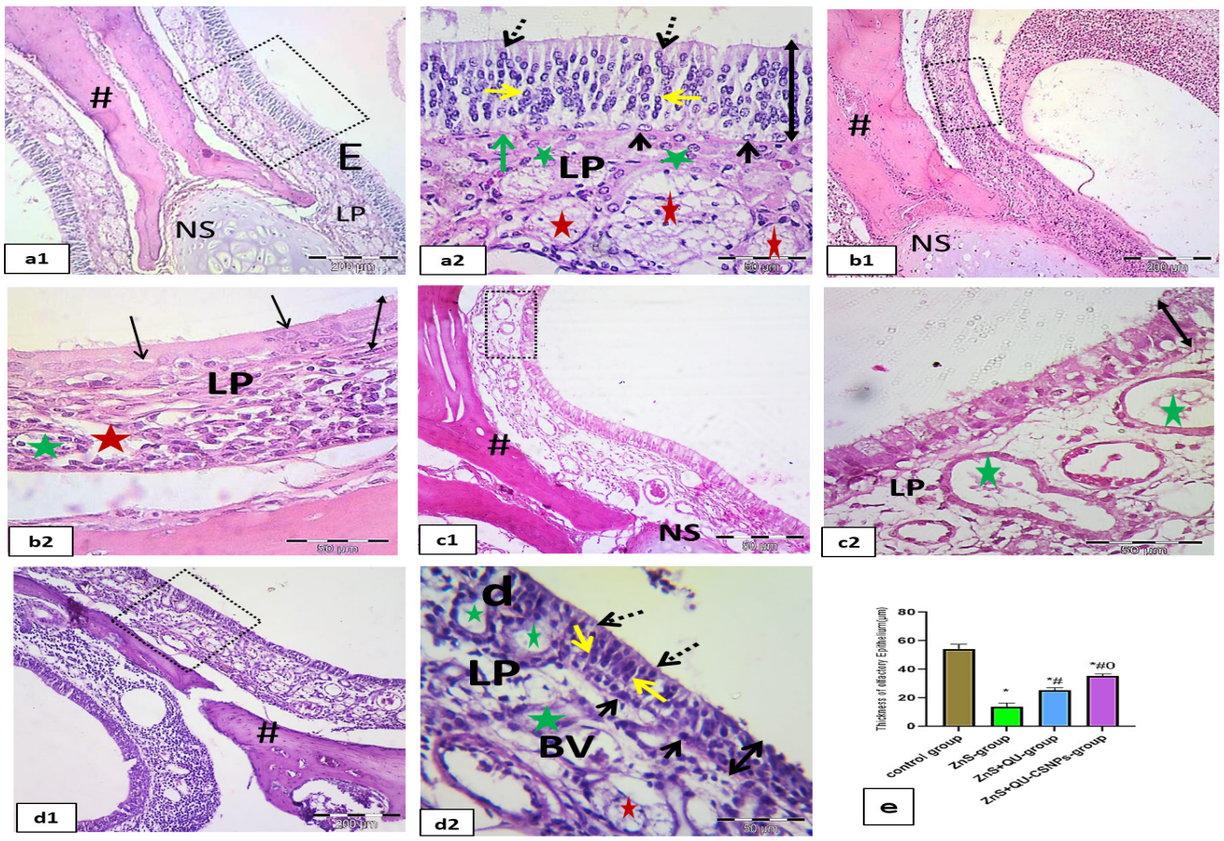

Figure 2: Photomicrographs of rat's olfactory mucosa of different groups: a) Control group showing: a1) Nasal bone (#) and nasal septum (NS). Notice the olfactory mucosa (rectangle) which is formed of olfactory epithelium (E) and lamina propria (LP). a2) A higher magnification of the rectangle showing olfactory epithelium (double- headed arrow) which is formed of three cell types, horizontal basal cells (black arrows), resting on basement membrane (green arrow), olfactory neurons (yellow arrows) and supporting cells (dotted arrows). Lamina propria (LP) showing Bowman's glands (green asterisks) and olfactory nerve bundles (red asterisks). b) ZnS –group showing b1) Damaged and apparently shrunken olfactory mucosa (rectangle). b2) A higher magnification showing preserved basal cells (arrows). The lamina propria (LP) showing degenerated nerve bundles (red asterisk) and damaged Bowman's glands with pyknotic nuclei, vacuolated cytoplasm and irregular outlines (green asterisk). c) ZnS+QU-group showing:c1 columnar ciliated epithelial cells in olfactory epithelium area with goblet cells. c2) A higher magnification of the square showing replacement of olfactory epithelial cells with columner ciliated cells (double -headed arrow). The lamina propria (LP) showing dilated Bowman's glands (green asterisks). d) ZnS+QU-CSNPs group showing: d1) Olfactory mucosa with apparently preserved epithelium. d2) A higher magnification of the square showing olfactory epithelium (double head arrow) with its cell types: supporting cells (dotted arrows), olfactory neurons (yellow arrows) and basal cells (black arrows). The lamina propria (LP) showing nerve bundle (red asterisk). Notice dilated Bowman's Gland (green asterisks) and dilated Blood vessel (B.V). e) The mean values of the olfactory epithelium thickness in different groups (n = 6). Significance: * vs control, # vs ZnS group, 0 vs ZnS+QU treated group. (H&E a1, b1, c1, d1 X100 , a2, b2, c2, d2 X 400. scale bar: a1, b1, c1, d1 =200 µm; scale bar: a2, b2, c2, d2 = 50 µm).

Olfactory bulb Hematoxylin and eosin results:

The control sections were consisted of six distinct layers, the olfactory nerve layer (ONL), contained the olfactory nerve fibers. The glomerular layer (GL) consisted of one row of glomeruli which were a cellular synaptic nearly spherical masses of varying sizes composed of fine fibrils and surrounded by small juxtaglomerular cells (Figure 3a1). The external plexiform layer (EPL), a thick layer consisted of fine nerve fibers, sparsely distributed tufted cells and interneurons (Figure 3a2). The mitral cell layer (MCL), a thin layer containing the somata of mitral cells arranged in a row. Mitral cells were triangular with acidophilic cytoplasm containing basophilic patches and large rounded vesicular nuclei (Figure 3a2). The internal plexiform layer (IPL), a thin layer composed of fine nerve fibers and some granule cells (Figure 3a2). The granule cell layer (GCL) contained large number of granule cells arranged in clusters, the granule cells were small cells with deeply

stained rounded nucleus and thin rim of cytoplasm (Figure 3a2). The ZnS group showed widely spaced distorted shape nerve fibers. There were dilated congested blood capillaries in the olfactory nerve layer (Figure 3b1). Mitral cells were small and darkly stained with pyknotic nuclei. Also, granule cells were small and darkly stained. Some mitral cells and granule cells showed pericellular hallows (Figure 3b2). The ZnS+QU treated group showed loss of the structural integrity of the olfactory nerve layer with widely spaced nerve fibers, periglomerular area and glomerular neuropil. The nerve fibers within glomeruli were less compacted (Figure 3c1). Some mitral cells were large with large rounded vesicular nuclei. While some others were small and darkly stained with pericellular hallows (Figure 3c2). The ZnS+QU-CSNPs treated group showed apparently normal architecture of olfactory bulb. The olfactory nerve fibers of ONL were less widely separated. Glomeruli of GL were spherical in shape and surrounded by juxtaglomerular cells, the nerve fibers within the glomeruli were compactly packed (Figure 3d1). Mitral cells were large with large rounded vesicular nuclei and granule cells were numerous and organized (Figure 3d2).

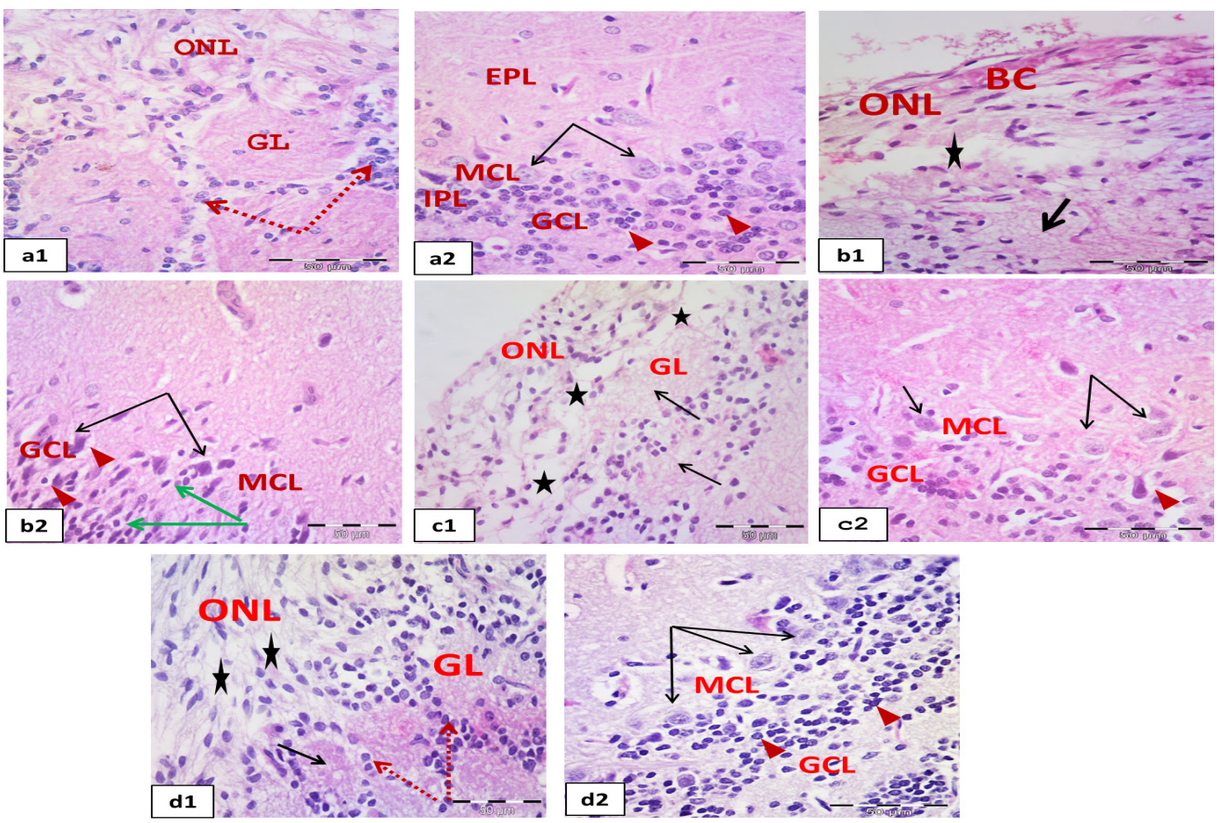

Figure 3: Photomicrographs of rat's olfactory bulb. a) Control group showing: a1) the layers of the olfactory bulb composed of the olfactory nerve layer (ONL) and glomerular layer (GL) which is formed of glomruli surrounded by juxtaglomerular cells (dotted arrows). a2) External plexiform layer (EPL), mitral cell layer (MCL), internal plexiform layer (IPL) and part of granule cell layer (GCL). MCL is formed of large mitral cells (arrows), closely related to granule cells (arrow heads). b) ZnS –group showing: b1) widely spaced nerve fibers in the olfactory nerve layer (asterisk). The nerve fibers within glomeruli are less compacted (arrow). Notice congested dilated blood capillaries in the olfactory nerve layer (BC). b2) Small darkly stained mitral cells with darkly stained nuclei and darkly stained cytoplasm (arrows), granule cells were darkly stained (green arrows), Some mitral cells and granule cells showing pericellular hallows (arrow heads). c) ZnS+QU-group showing:c1) widely spaced nerve fibers in the olfacotory nerve layer (ONL) (asterisks), The nerve fibers within glomeruli are less compacted (arrows). c2) Large mitral cells with large rounded vesicular nuclei (arrows). Some mitral cells are small and darkly stained with pericellular hallows (arrowhead). d) ZnS+QU-CSNPs group showing: d1) olfactory nerve fibers of olfactory nerve layer (ONL) are less widely separated (asterisks) with spherical shape glomeruli (GL) which are surrounded by juxtaglomerular cells (dotted arrows). The nerve fibers within the glomeruli are compactly packed (arrow). d2) Large mitral cells with large rounded vesicular nuclei (arrows). Notice the organized granule cells (arrow heads). (H&E a1, b1, c1, d1 X100, a2, b2, c2, d2 X 400. scale bar: a1, b1, c1, d1 =200 µm; scale bar: a2, b2, c2, d2 = 50 µm).

Alcian blue-periodic acid Schiff stain results:

Olfactory mucosa of control group showed positive reaction of Bowman's glands contents and in intraepithelial duct (Figure 4a), in contrast ZnS group revealed faint positive reaction of Bowman's glands contents (Figure 4b). While ZnS+QU treated group showed apparent more reaction of Bowman's glands contents than ZnS group (Figure 4c). Meanwhile, it was noticed in ZnS+QU-CSNPs treated group more positive reaction of Bowman's glands contents and in intraepithelial duct than previous group (Figure 4d).

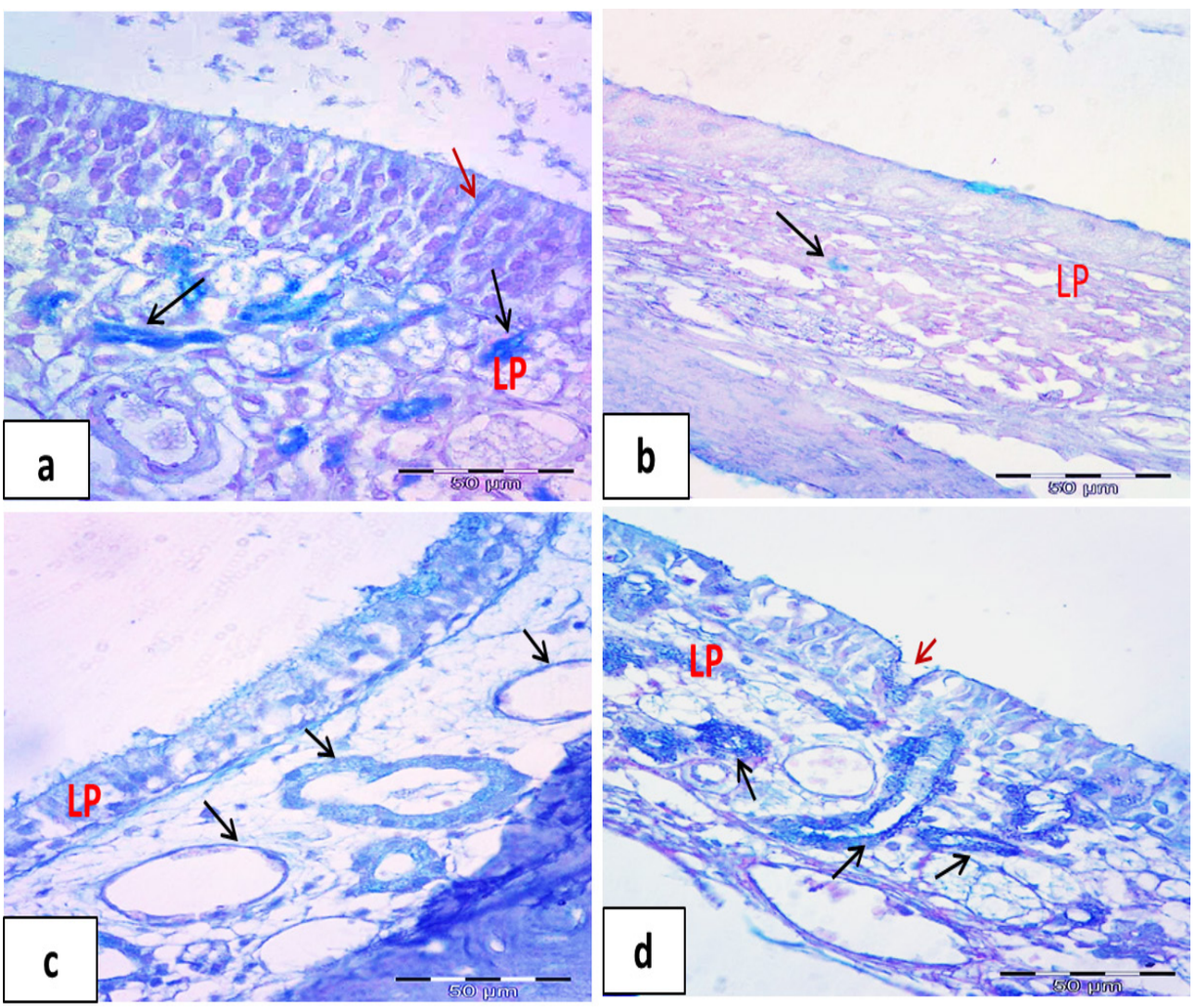

Figure 4: Photomicrographs of rat's olfactory mucosa stained with Alcian Blue Periodic Acid Schiff of: a) Control group showing strong positive reaction of Bowman's glands contents (black arrows) and intraepithelial duct (red arrow). b) ZnS group showing faint reaction of Bowman's glands contents (black arrows). c) ZnS+QU group showing more positive reaction of Bowman's glands contents (arrows). d) ZnS+Q-CSNPs group showing apparent more positive reaction of Bowman's glands contents (arrows) and of intraepithelial duct (red arrow) than previous group. (Alcian Blue-Periodic Acid Schiff stain: X 400; scale bar = 50 µm).

Immunohistochemical results:

Regarding olfactory mucosa, the control group showed positive SOX2 nuclear immunoexpression in some basal cells and supporting cells (Figure 5a). ZnS group showed positive SOX2 nuclear immunoexpression in few basal cells (Figure 5b). ZnS+QU treated group showed apparent more positive SOX2 nuclear immunoexpress ion in few basal cells than noticed in previously group (Figure 5c). While ZnS+QU-CSNPs treated group showed more positive extensive SOX2 nuclear immunoexpression in more basal cells (arrows) and supporting cells (Figure 5d) than previous group.

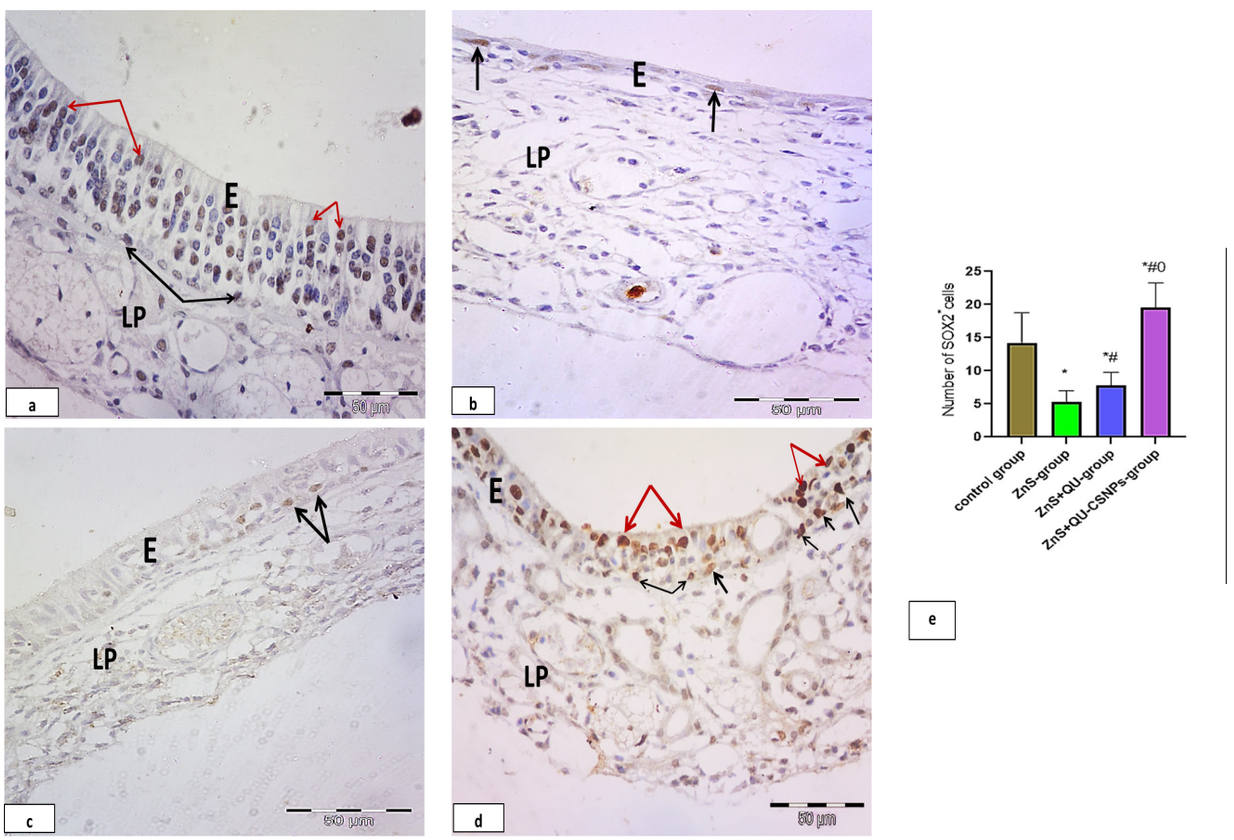

Figure 5: Photomicrographs of rat olfactory mucosa immunostained with SOX2 of: a) Control group showing positive SOX2 nuclear immunoexpression in some basal cells (black arrows) and supporting cells (red arrows). b) ZnS group showing positive SOX2 nuclear immunoexpression in few basal cells (arrows). c) ZnS +QU group showing apparent more positive SOX2 nuclear immunoexpression in few basal cells (arrows). d) ZnS +QU-CSNPs group showing more extensive positive SOX2 nuclear immunoexpression in basal cells (black arrows) and supporting cells (red arrows). e) The mean number of SOX2 immunopositive cells in olfactory mucosa in different groups (n=6). Significance: * vs control, # vs ZnS group, 0 vs ZnS+QU treated group. (IHC- SOX2, H x 400; scale bar = 50 µm)

Regarding olfactory mucosa, control group showed positive PCNA nuclear immunoexpression in some olfactory epithelial layer and lamina propria (Figure 6a). While ZnS group showed positive nuclear immunoexpression in few olfactory epithelial layer and lamina propria cells (Figure 6b). The ZnS+QU treated group showed positive PCNA nuclear immunoexpression in a few olfactory epithelial layer and lamina propria cells (Figure 6c). The ZnS+QU-CSNPs treated group showed positive PCNA nuclear immunoexpression in more olfactory epithelial layer and lamina propria cells (Figure 6d).

As regard olfactory bulb, control group positive PCNA nuclear immunoexpression in some ONL and GL with negative expression in EPL (Figure 7a) while Rostral migratory stream (RMS) showed few PCNA immunopositive cells in elbow and horizontal regions (Figures 8a and 9a). ZnS group showed positive PCNA nuclear immunoexpression in few cells of ONL (Figure 7b) while RMS showed positive PCNA nuclear immunoexpression in few cells of elbow region and negative PCNA nuclear immunoexpressing cells in horizontal region (Figures 8b and 9b).

ZnS+QU treated group showed positive PCNA nuclear immunoexpression in many cells of ONL, GL and EPL (Figure 7c). RMS showed positive PCNA nuclear immunoexpression in many cells of elbow and horizontal regions (Figures 8c and 9c). ZnS+QU-CSNPs treated group showed more positive PCNA nuclear immunoexpression cells of ONL, GL, EPL and GL (Figure 7d). RMS showed positive PCNA nuclear immunoexpression in many cells of elbow and horizontal regions (Figures 8d and 9d).

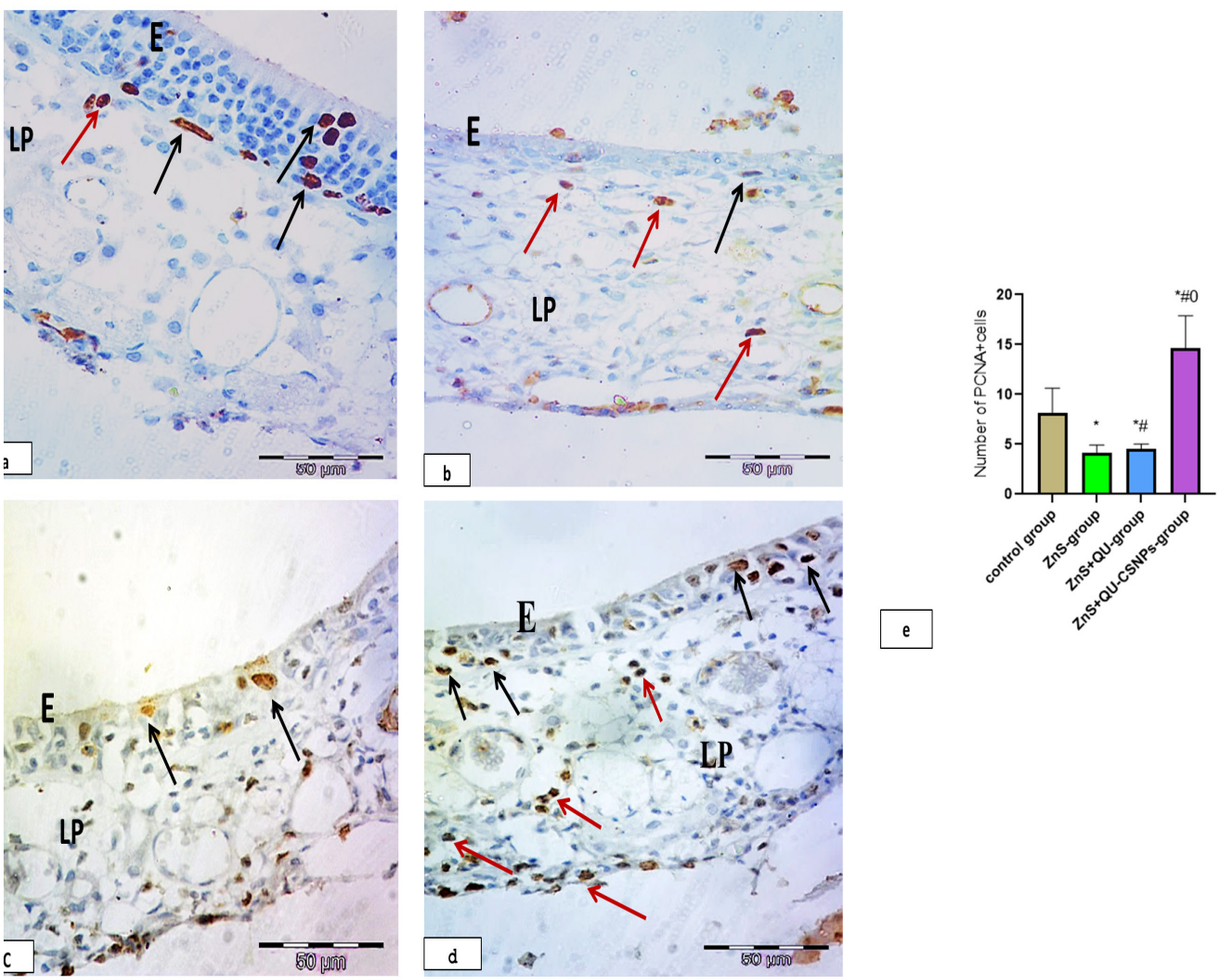

Figure 6: Photomicrographs of rat's olfactory mucosa immunostained with PCNA in diffirent groups showing: a) Control group showing positive PCNA nuclear immunoexpression in some olfactory epithelial layer (E) (black arrows) and lamina propria cells (LP) (red arrow). b) ZnS group showing positive PCNA nuclear immunoexpression in few olfactory epithelial layer (E) (black arrows) and lamina propria cells (LP) (red arrows). c) ZnS+QU group showing positive PCNA nuclear immunoexpression in few olfactory epithelial layer cells (E) (black arrows). d) ZnS+QU-CSNPs group showing more positive PCNA nuclear immunoexpression in olfactory epithelial layer (E) (black arrows) and lamina propria cells (LP) (red arrows). e) The mean number of PCNA immunopositive cells in olfactory mucosa in different groups (n = 6). Significance: * vs control, # vs ZnS group, 0 vs ZnS+QU treated group. (IHC- PCNA, H a, b, c, d x400, scale bar: a, b, c, d = 50 µm).

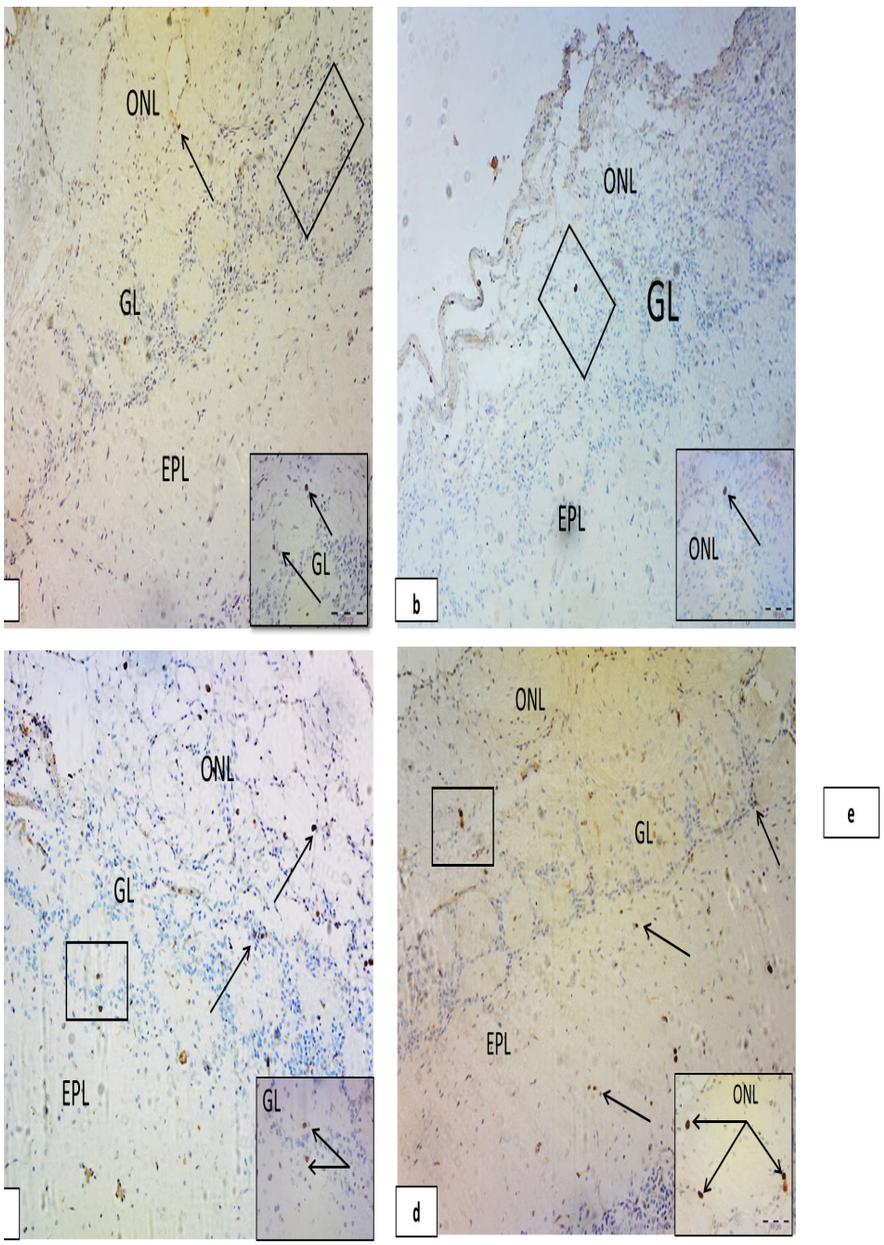

Figure 7: Photomicrographs of rat's olfactory bulb immunostained with PCNA in diffirent groups showing: a) Control group showing positive PCNA nuclear immunoexpression in some cells of olfactory nerve layer (ONL) (arrow) and glomerular layer (GL) (square). Inset showing PCNA positive cells in glomerular layer (GL) (arrows) with negative expression in external plexiform layer (EPL). b) ZnS group showing positive PCNA nuclear immunoexpression in few cells of olfactory nerve layer (ONL) (square). Inset is a higher magnification of the square showing PCNA positive cell in ONL. c) ZnS+QU group showing positive PCNA nuclear immunoexpression in many cells of olfactory nerve layer (ONL) (arrows), glomerular layer (GL) and external plexiform layer (EPL) (square). Inset is a higher magnification of the square showing PCNA positive cells in glomerular layer(GL) and external plexiform layer (EPL) (arrows). d) ZnS+QU-CSNPs group showing positive PCNA nuclear immunoexpression in many cells of olfactory nerve layer (ONL) (square), glomerular layer (GL), and external plexiform layer (EPL) (arrows). Inset is a higher magnification of the square showing Positive PCNA nuclear immunoexpression in cells of olfactory nerve layer (ONL) (arrows). e) The mean number of PCNA immunopositive cells in olfactory bulb in different groups (n = 6). Significance: * vs control, # vs ZnS group, 0 vs ZnS+QU treated group. (IHC- PCNA, H a, b, c, d X100, insets X 400; scale bar: a, b, c, d = 200 µm; scale bar: insets = 50 µm).

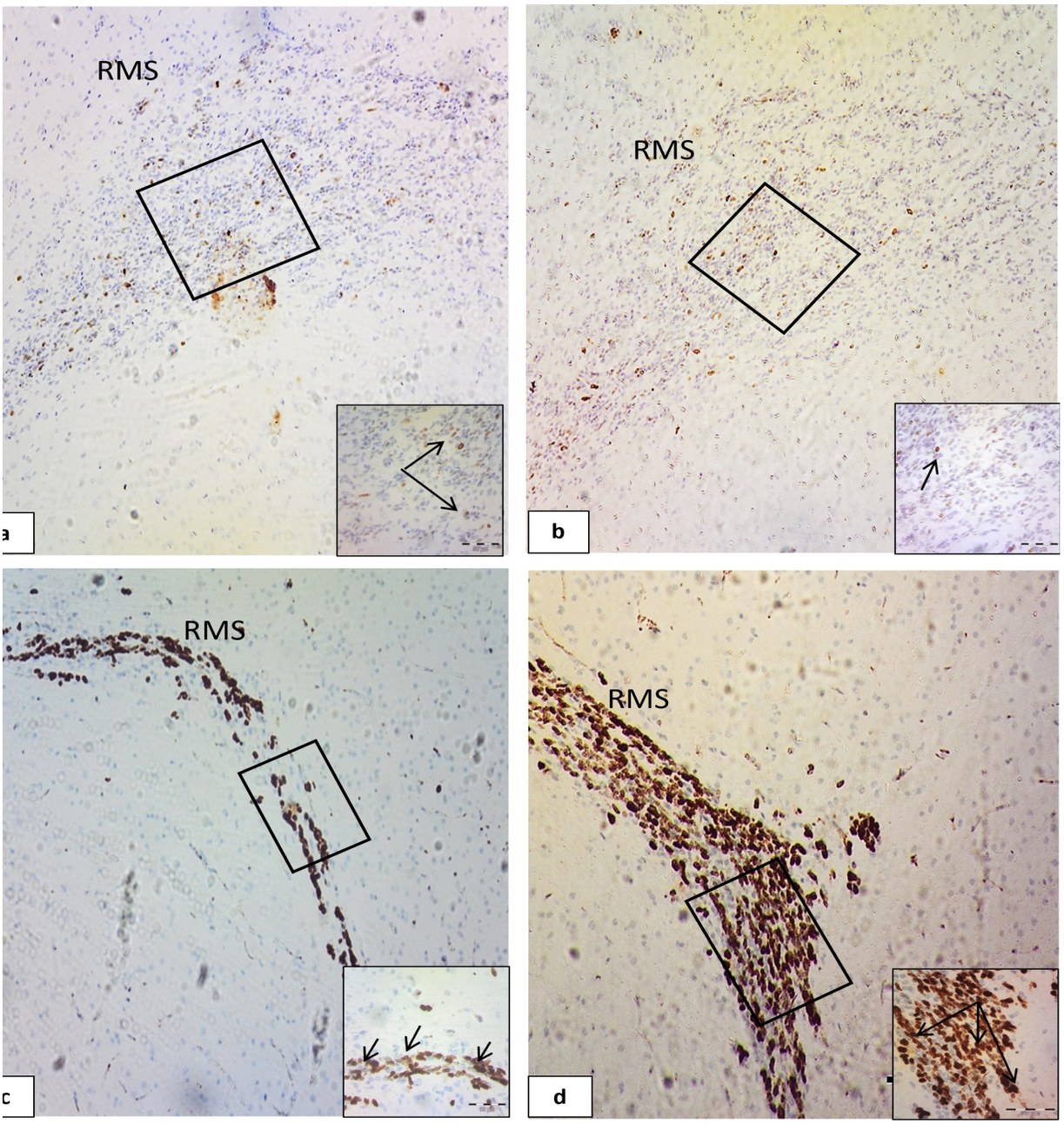

Figure 8: Photomicrographs of rat's elbow region of rostral migratory stream (RMS) immunostained with PCNA in diffirrent groups showing: a) Control group showing few PCNA positive cells in elbow region (square). Inset is a higher magnification of the square showing PCNA positive nuclear expression cells (arrows). b) ZnS –group showing few PCNA positive cells in elbow region (square). Inset is a higher magnification of the square showing PCNA positive nuclear expression cells (arrows). c) ZnS+QU group showing numerous PCNA positive cells in elbow region (square). Inset is a higher magnification of the square showing PCNA positive nuclear expression cells (arrows). d) ZnS+QU-CSNPs group showing more numerous PCNA positive cells in elbow region (square). Inset is a higher magnification of the square showing PCNA positive cells (arrows). (IHC- PCNA a, b, c, d X100, insets X 400; scale bar: a, b, c, d = 200 µm; scale bar: insets = 50 µm).

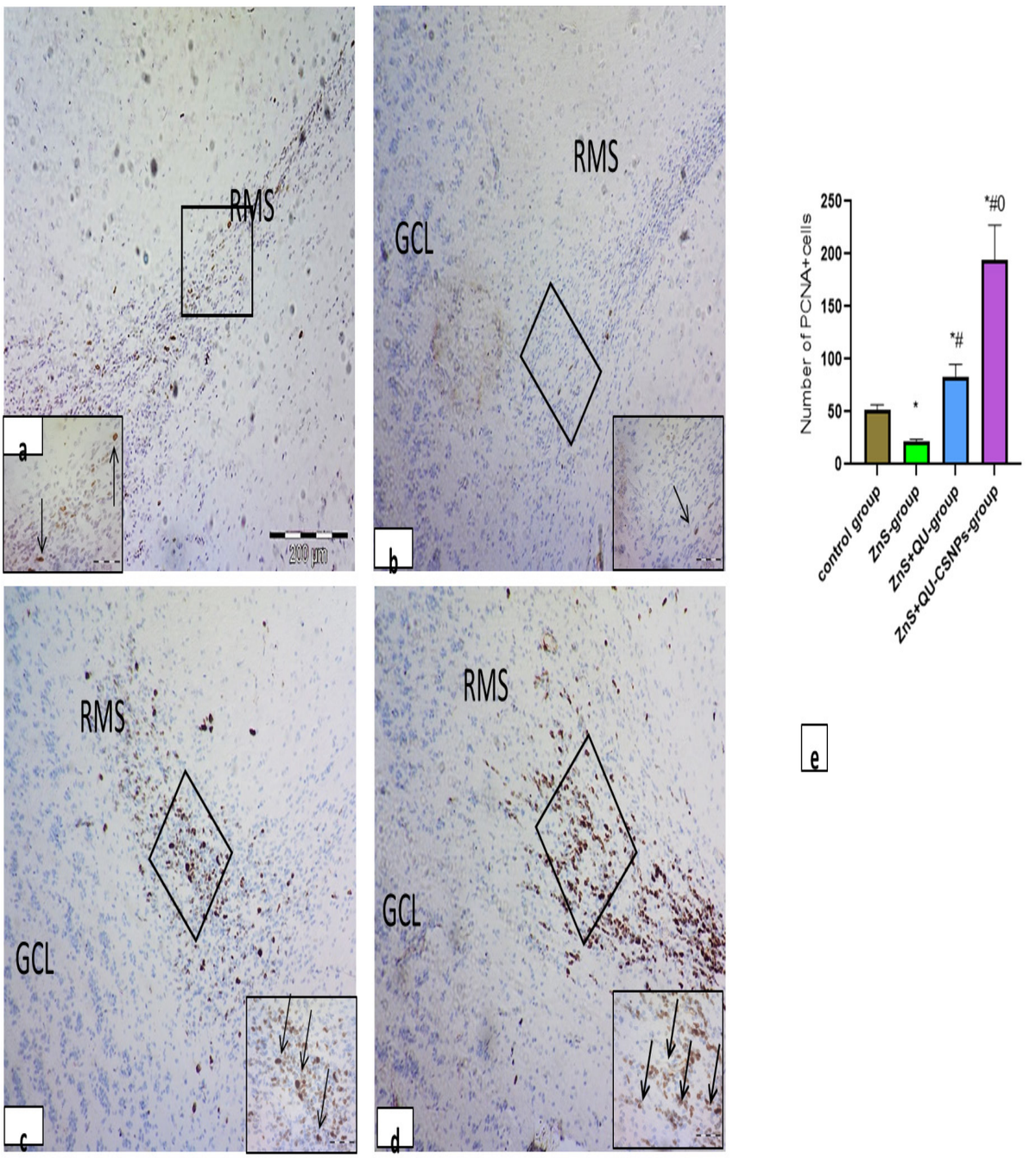

Figure 9: Photomicrographs of rat's horizontal region of rostral migratory stream (RMS) immunostained with PCNA in diffirrent groups showing: a) Control group showing few PCNA positive nuclear expression cells in horizontal region (square). Inset is a higher magnification of the square showing PCNA positive nuclear expression cells (arrows). b) ZnS –group showing PCNA expression cells in few cells in horizontal region (square). Inset is a higher magnification of the square. c) ZnS+QU- group showing numerous PCNA positive nuclear expression cells in horizontal region (square). Inset is a higher magnification of the square showing numerous PCNA positive nuclear expression cells (arrows). d) ZnS+QU-CSNPs group showing numerous PCNA positive cells in horizontal region (square). Inset is a higher magnification of the square showing numerous PCNA positive cells (arrows). e) The mean number of PCNA immunopositive cells in Rostral migratory stream in different groups (n = 6). Significance: * vs control, # vs ZnS group, 0 vs ZnS+QU group. (IHC-PCNA a, b, c, d X100, insets X 400; scale bar: a, b, c, d = 200 µm; scale bar: insets = 50 µm).

Regarding olfactory mucosa, control group showed negative COX2 cytoplasmic immunoexpression (Figure 10a). While ZnS group showed strong COX2 cytoplasmic immunoexpression in olfactory epithelial cells (Figure 10b). It was noticed in ZnS+QU treated group showed strong COX2 cytoplasmic immunoexpression in some olfactory epithelial cells (Figure 10c). ZnS+QU-CSNPs treated group showed faint COX2 cytoplasmic immunoexpression in olfactory epithelial cells (Figure 10d). As regard olfactory bulb, Control group showed negative COX2 cytoplasmic immunoexpression in ONL, GL, EPL and MCL (Figures 11a1 and 11a2). ZnS group showed strong COX2 cytoplasmic immunoexpression in ONL, GL, EPL and some mitral cells (Figures 11b1 and 11b2). ZnS+QU treated group showed weak COX2 cytoplasmic immunoexpression in ONL, GL, EPL and some mitral cells (Figures 11c1 and 11c2). ZnS+QU-CSNPs treated group showed faint COX2 cytoplasmic immunoexpression in ONL, GL, EPL and MCL (Figures 11d and 11d).

Semithin sections results:

Olfactory epithelium of control group formed of supporting cells, olfactory neurons and basal cells. Lamina propria showed Bowman's glands with radial orientation of acinar cells (Figure 12a) while ZnS group displayed damaged epithelium. Inflammatory cells in nasal cavity were noticed (Figure 12b). It was noticed in ZnS+QU group a replacement of olfactory epithelial cells with columnar ciliated cells (Figure 12c). ZnS+QU-CSNPs group showed supporting cells, olfactory neurons and basal cells. Intraepithelial duct of Bowman's gland (D) and excretory duct cells were noticed. Lamina propria showed Bowman's glands with radial orientation of acinar cells. (Figure 12d). Regarding Bowman's glands, control group showed acini Bowman's glands in lamina propria which were radially oriented around the lumen with secretory granules (Figure 13a). ZnS group showed loss of radial orientation of acinar cells of Bowman's gland with vacuolated cytoplasm, small, dense and dark shrunken nuclei and dispersed secretory granules (Figure 13b). ZnS+QU treated group showed some acinar cells which were shrunken and darkly stained with loss of radial orientation (Figure 13c). ZnS+QU-CSNPs treated group revealed restoration of normal appearance of acinar cells which were radially oriented around the lumen with secretory granules (Figure 13d). Regarding olfactory bulb, control group showed the mitral nerve cells having large vesicular nuclei with prominent nucleoli and granule cells with large central nucleus and surrounded with thin rim of cytoplasm (Figure 13e). ZnS group showed shrinking of mitral cells, cytoplasmic vacuolations of granule cells. The surrounding neuropil appeared with vacuolations (Figure 13f). ZnS+QU treated group showed some apparently normal mitral cells, but others were shrunken and dark. Granule cells were having normal appearance (Figure 13g). ZnS+QU-CSNPs treated group showed restored apparent normal mitral cells and granule cells with intact neuropil (Figure 13h).

Transmission electron microscopic results:

As regard olfactory mucosa, control group showed the acinar cells of the Bowman's gland that were clearly distinguishable with their regular radial organization around a lumen. There were microvilli on the luminal surface of acinar cells; the cytoplasm was dense containing secretory granules of different electron density. The acinar cells in the lamina propria also contained a large amount of homogeneously electron-dense mitochondria that were in contact with r-ER (Figure 14a). ZnS group showed acinar cells of Bowman's gland with vacuolated cytoplasm, dilated r-ER cisternae. Secretory granules were few and disrupted (Figure 14b). ZnS+QU treated group showed acinar cells with peripheral heterochromatic chromatin and dilated r-ER cisternae (Figure 14c). ZnS+QU-CSNPs treated group showed restoration of acinar cell ultrastructure in the form of regular nucleus, electron dense cytoplasm, apparently normal cisternae of r-ER and secretory granules and presence of microvilli on the luminal surface of acinar cells (Figure 14d). Regarding olfactory bulb, mitral nerve cells of control group appeared with scanty cytoplasm and heterochromatic large nuclei (Figure 15a). ZnS group revealed many degenerative changes including densely stained cytoplasm with vacuolations, irregular nuclei and dilated Golgi apparatus (Figure 15b).

ZnS+QU treated group showed partial restoration of ultrastructure of mitral nerve cells (Figure 15c). ZnS+QU-CSNPs treated group showed apparently normal mitral nerve cells with euchromatic nucleus and dispersed chromatin, abundant cytoplasm rich in r-ER and mitochondria (Figure 15d). Granule cells of control group appeared with scanty cytoplasm and heterochromatic large nuclei (Figure 15e). ZnS group showed cytoplasmic vacuolation of granule cells and surrounding neuropil showed splitting of myelin sheath of axons (Figure 15f). ZnS+QU treated group showed more or less normal granule cells (Figure 15g). ZnS+QU-CSNPs treated group showed apparent normal ultrastructure appearance of granule cells with large nucleus and densely packed chromatin and surrounded by thin rim of cytoplasm

(Figure 15h). The Myeline sheath of control group showed intact myelin sheath with compact myelin lamellae (Figure 16a). Myelin sheath of ZnS group showed changes in the form of splitting, irregular outline with axoplasm and neuropil vacuolation (Figure 16b). ZnS+QU treated group showed intact myelin sheath (Figure 16c). ZnS+QU-CSNPs treated group revealed intact myelin sheath with intact surrounding neuropil (Figure 16d).

Morphometric results:

All morphometric results were shown in the form of histogram in Figures 2e, 5e, 6e, 7e, 9e, 10e, 11e, Tables 4 and 5.

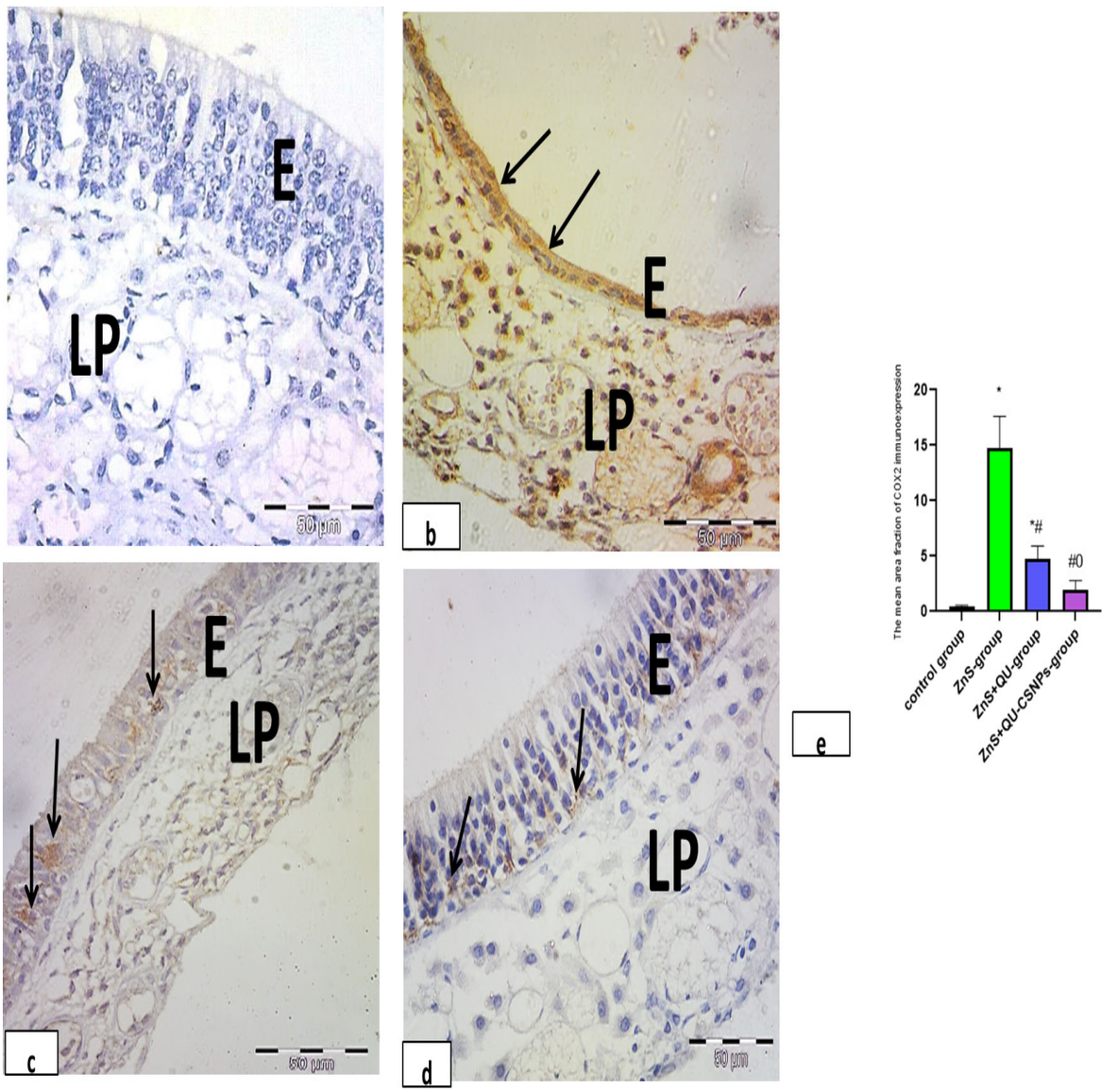

Figure 10: Photomicrographs of rat olfactory mucosa immunostained with COX-2 in diffirent groups showing: a) Control group showing negative COX2 cytoplasmic immunoexpression. b) ZnS – group showing strong COX2 cytoplasmic immunoexpression in olfactory epithelial cells (arrows). c) ZnS+QU group showing COX2 cytoplasmic immunoexpression in some olfactory epithelial cells (arrows). d) ZnS+QU-CSNPs group showing faint COX2 cytoplasmic immunoexpression in olfactory epithelia cells (arrows). e) The mean values of COX2 area fraction in olfactory mucosa in different groups (n = 6). Significance: * vs control, # vs ZnS group, 0 vs ZnS+QU group. (IHC-COX2 a,b,c,d X 400; scale bar: a, b, c, d = 50 µm).

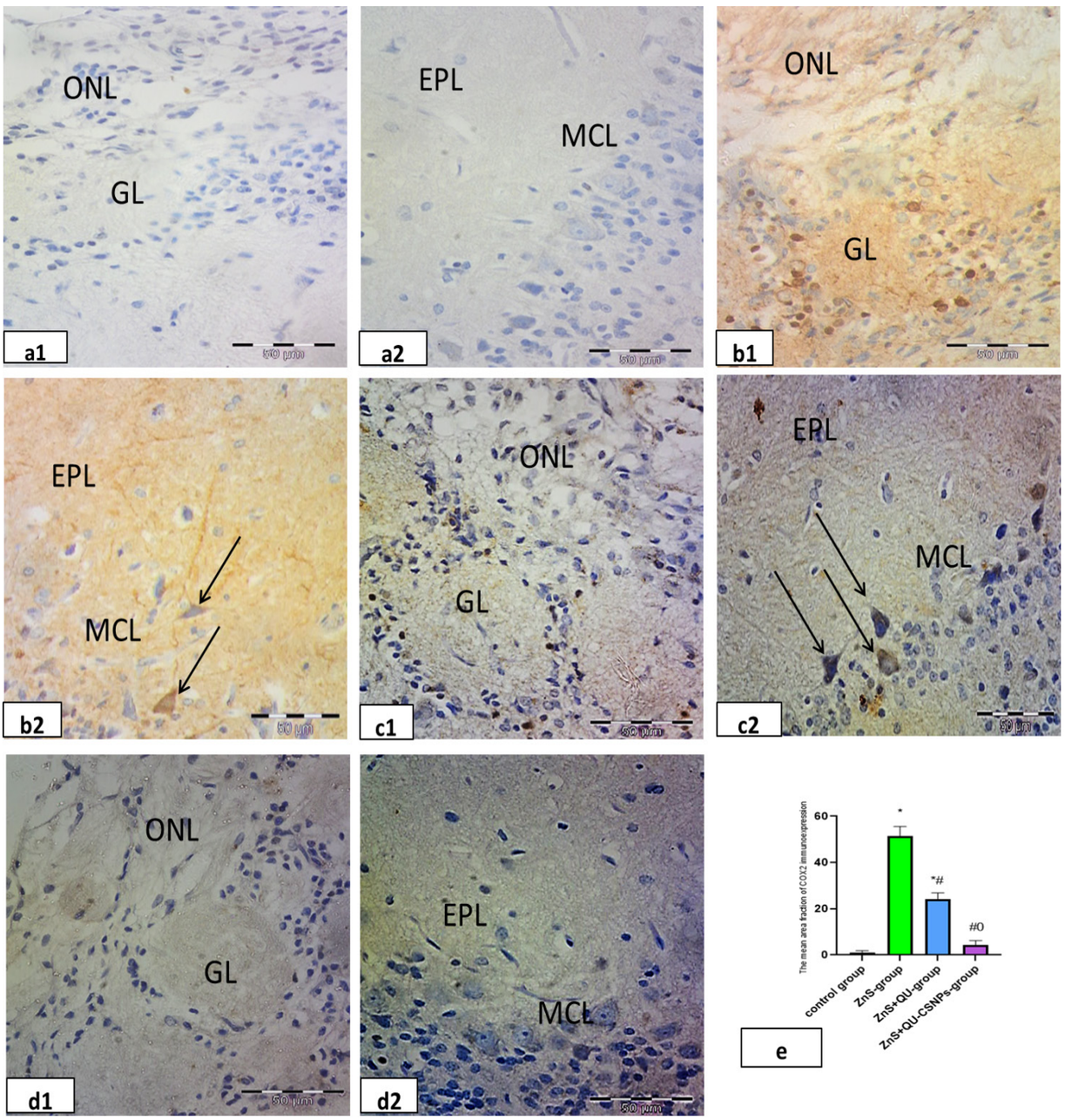

Figure 11: P Photomicrographs of rat olfactory bulb immunostained with COX-2 in diffirent groups. a) Control group. a1) showing negative COX-2 expression in olfactory nervre layer (ONL) and glomerular layer(GL). a2) Control group showing negative COX-2 expression in external plexiform layer (EPL) and mitral cell layer (MCL). b) ZnS –group showing b1) strong COX-2 expression in olfactory nerve layer (ONL) and glomerular layer(GL). b2) showing strong COX-2 expression in external plexiform layer (EPL) and cytoplasm of some mitral cells (arrows). c) ZnS+QU group showing c1)weak COX-2 expression in olfactory nerve layer (ONL) and glomerular layer(GL). c2) showing weak COX-2 expression in external plexiform layer (EPL) and cytoplasm of some mitral cells (arrows). d) ZnS+QU-CSNPs group. d1)faint COX-2 expression in olfactory nerve layer (ONL) and glomerular layer (GL). d2) Showing faint COX-2 expression in external plexiform layer (EPL) and mitral cell layer (MCL). e) The mean values of COX2 area fraction in olfactory bulb in different groups (n = 6). Significance: * vs control, # vs ZnS group, 0 vs ZnS+QU group. (IHC-COX2 a, b, c, d X 400; scale bar: a, b, c, d = 50 µm).

Table 4: The mean values of the olfactory epithelium thickness in different groups (n = 6):

Groups	Mean ± SD	*P* value
Control group	54.21 ± 3.47	
ZnS group	13.64 ± 2.75	<0.000c*
ZnS+QU treated group	25.43 ± 1.74	<0.000c* <0.000Z*
ZnS+QU-CSNPs treated group	35.50 ± 1.34	<0.000c* <0.000Z* <0.000Z+Q*

C versus the control group, Z versus ZnS and Z+Q versus ZnS+QU treated group.
*$P < 0.05$ is significant.

Table 5: The mean number of SOX2, PCNA, COX2 in immunopositive cells in olfactory mucosa and olfactory bulb in different groups (n = 6):

Groups	The mean number of SOX2 immunopositive cells in olfactory mucosa		The mean number of PCNA immunopositive cells in olfactory mucosa		The mean number of PCNA immunopositive cells in olfactory bulb		The mean number of PCNA immunopositive cells in rostral migratory stream		The mean values of COX2 area fraction in olfactory mucosa		The mean values of COX2 area fraction in olfactory bulb	
G	Mean ± SD	*P* value	Mean ± SD	*P* value	Mean ± SD	*P* value	Mean ± SD	*P* value	Mean ± SD	*P* value	Mean ± SD	*P* value
Control group	14.17 ± 4.62		8.16 ± 2.48		3.83 ± 1.16		52.00 ± 4.60		0.44 ± 0.10		1.19 ± 0.69	
ZnS group	5.33 ±1.63	0.000c*	4.16 ± 0.75	0.016c*	1.66 ± 0.81	0.027c*	21.67 ± 2.16	0.035c*	14.78 ± 2.83	< 0.000c*	51.34 ± 4.25	< 0.000c*
ZnS+QU treated group	7.83 ±1.94	0.041c* 0.552Z	4.50 ± 0.54	0.029c* 0.992Z	6.00 ± 0.89	0.022c* < 0.000Z	83.67 ± 12.33	0.027c* < 0.000Z*	4.71 ± 1.19	< 0.000c* < 0.000Z*	24.03 ± 2.86	< 0.000c* < 0.000Z*
ZnS+QU-CSNPs treated group	19.50 ± 3.78	0.045c* < 0.000Z* < 0.000Z+Q*	14.67 ± 3.20	0.000c* < 0.000Z* < 0.000Z+Q*	12.67 ± 1.75	< 0.000c* < 0.000Z* < 0.000Z+Q*	194.20 ± 33.23	< 0.000c* < 0.000Z* < 0.000Z+Q*	1.96 ± 0.80	0.370c < 0.000Z* 0.033Z+Q*	4.45 ± 1.81	0.200c < 0.000Z* < 0.000Z+Q*

C versus the control group, Z versus ZnS group and Z+Q versus the Q - treated group.*$P < 0.05$ is significant.

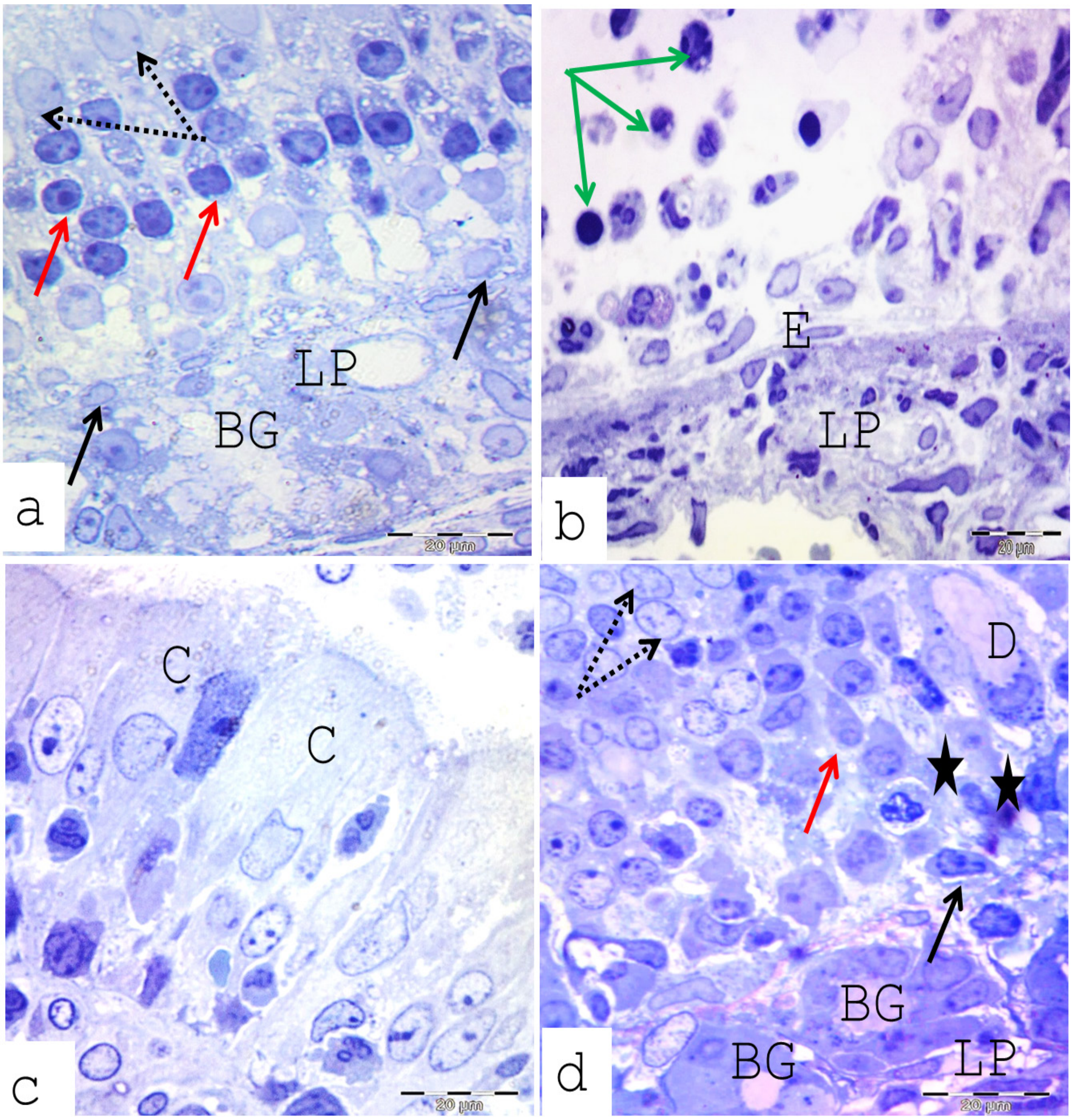

Figure 12: Photomicrographs of semithin sections of the rat's olfactory mucosa in different groups:a) Control group showing supporting cells (dashed arrows), olfactory neurons (red arrows) and basal cells(arrows). Lamina propria (LP) shows Bowman's glands (BG) with radial orientation of acinar cells. b) ZnS group showing damaged epithelium (E). Notice inflammatory cells in nasal cavity (green arrows). c) ZnS+QU group showing replacement of olfactory epithelial cells with columner ciliated cells (C). d) ZnS+QU-CSNPs group showing supporting cells (dashed arrows), olfactory neurons (red arrow) and basal cells (arrow). Notice intraepithelial duct of Bowman's gland (D) and excretory duct cells (asterisks). Lamina propria (LP) showing Bowman's glands (BG) with radial orientation of acinar cells. (Toluidine blue X 1000; scale bar = 20 µm).m).m).

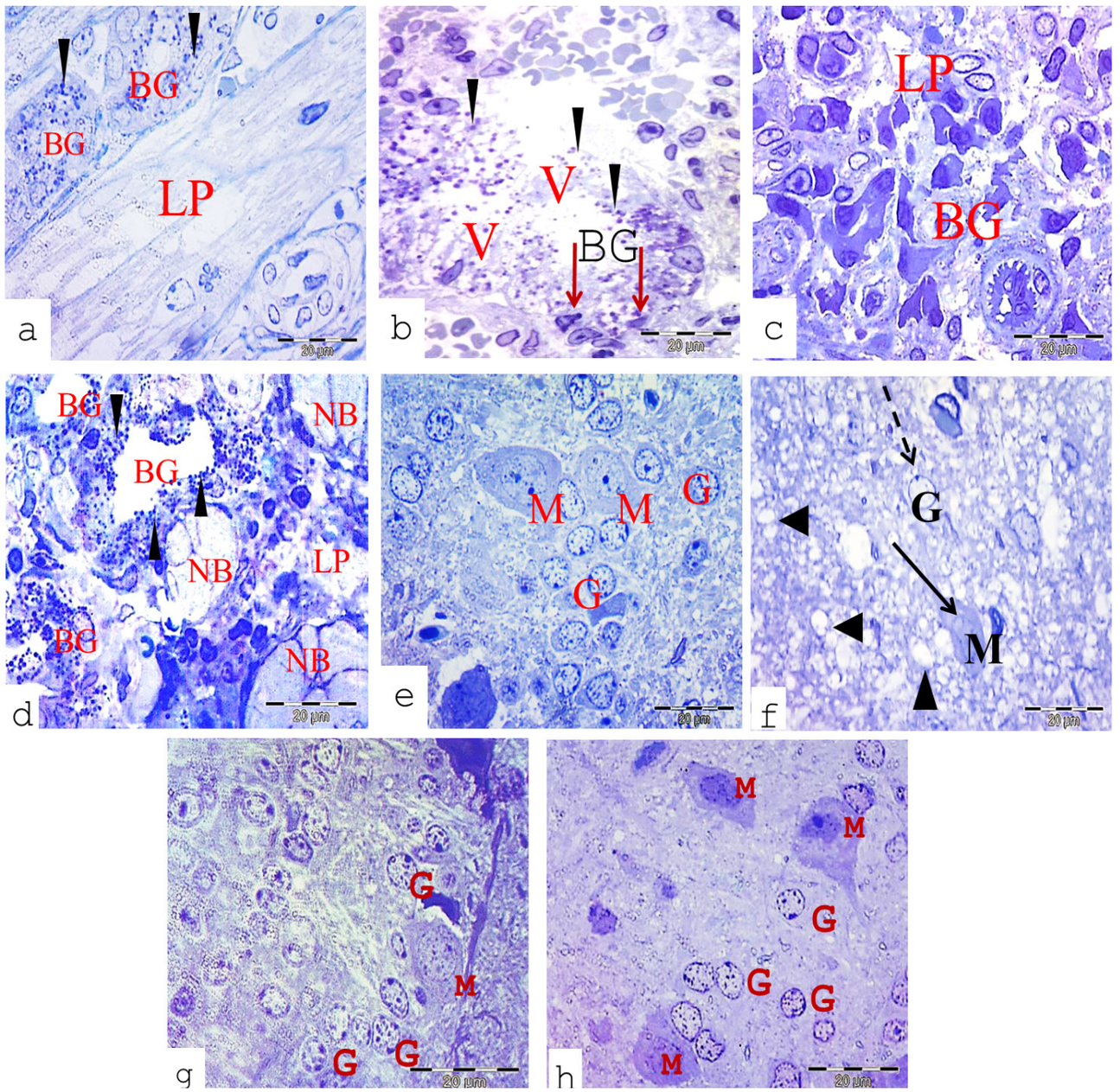

Figure 13: Photomicrographs of semithin sections of the rat's olfactory mucosa. a) Control group showing lamina propria (LP) with acini of Bowman's glands (BG) which are radially oriented around the lumen with secretory granules (arrow heads). b) ZnS –group showing loss of radial orientation of acinar cells of Bowman's Gland (BG) with vacuolated cytoplasm(V), small, dense and dark shrunken nuclei (red arrows) and dispersed secretory granules (arrow heads). c) ZnS+ QU- group showing lamina propria (LP) with shrunken darkly stained acini of Bowman's gland (BG) with loss of granules. d) ZnS+QU-CSNPs group showing lamina propria (LP) with nerve bundles (NB) and acini of Bowman's glands (BG) which are radially oriented around the lumen with secretory granules (arrow heads). e) Control group showing the mitral cells (M) having abundant cytoplasm and large lightly stained vesicular nuclei with prominent nucleoli located in the MCL. Granule cells (G) have large central nucleus and surrounded with thin rim of cytoplasm. f) ZnS group showing shrunken mitral cell (M) (arrow), granule cell (G) showing vaculations in its cytoplasm (dashed arrow). Notice vacuolations in neuropil (arrow heads). g) ZnS+QU group showing mitral cell (M) having abundant cytoplasm and large lightly stained vesicular nucleus granule cells have large central nucleus and surrounded with thin rim of cytoplasm (G). h) ZnS+QU-CSNPs group showing mitral cell (M) having abundant cytoplasm and large lightly stained vesicular nucleus, granule cells (G) have large central nucleus and surrounded with thin rim of cytoplasm. (Toludine blue X 1000; scale bar = 20 µm).

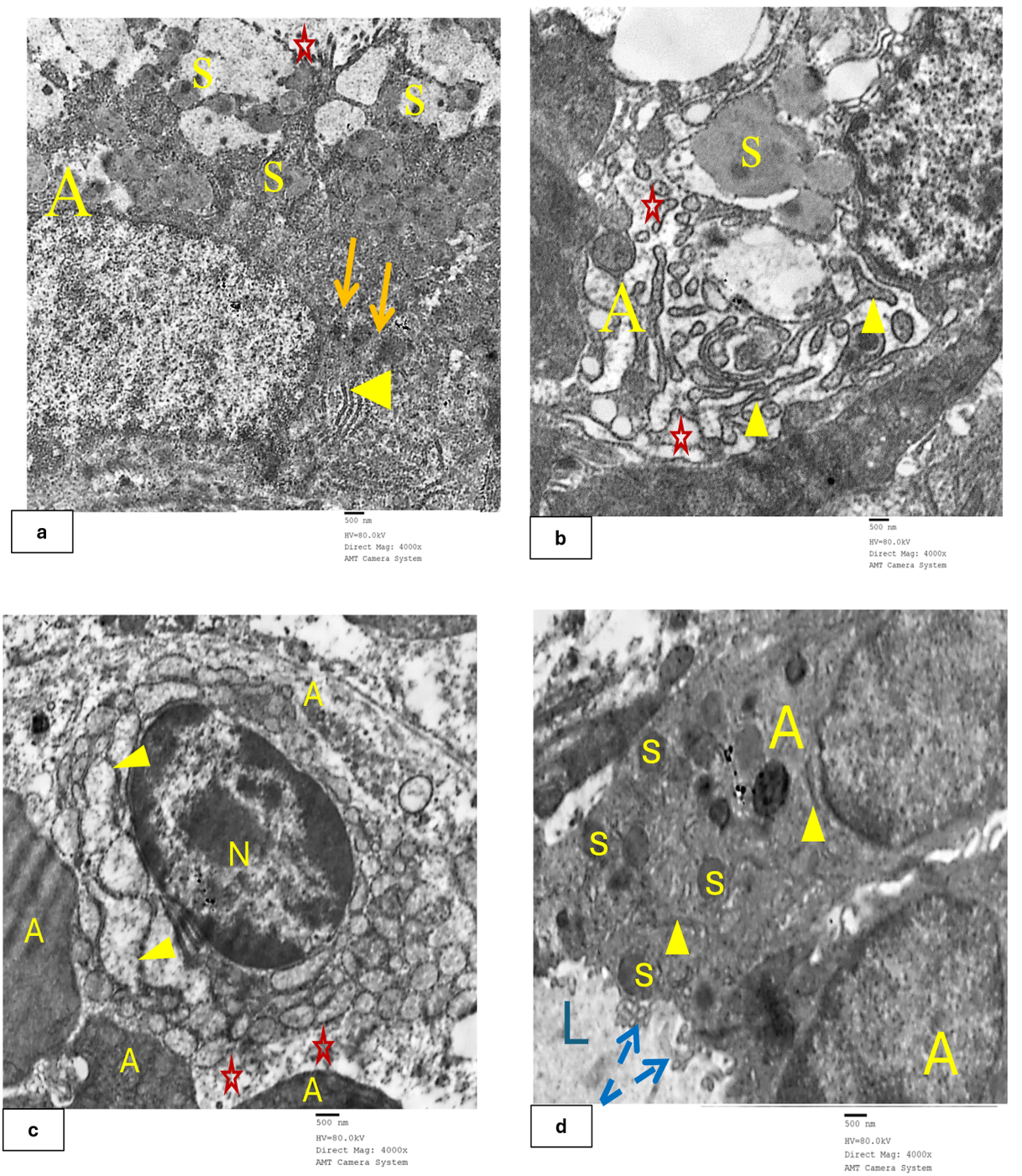

Figure 14: Electronmicrographs of the rat's Bowman's gland in different groups showing: a) Control group showing the acinar cell of Bowman's gland (A). The cytoplasm is dense containing secretory granules (S) of different electron density. The acinar cells contain a large amount of homogeneously electron-dense mitochondria (arrows) that are in contact with r-ER (arrow head). Notice micrvilli on the luminal surface (star). b) ZnS group showing acinar cell (A) of Bowman's gland with vacuolated cytoplasm (stars), dilated r-ER cisternae (arrow heads). Notice few secretory granules (s). c) ZnS+QU group showing an acinar cell with (star), heterochromatic nucleus (N) and dilated r-ER cisternae (arrow heads). d)ZnS+QU-CSNPs group showing an acinar cell (A) with regular nucleus, electron dense cytoplasm and secretory granules (S). There are microvilli on the luminal surface (L) of acinar cell (blue arrows). (TEM: X4000).

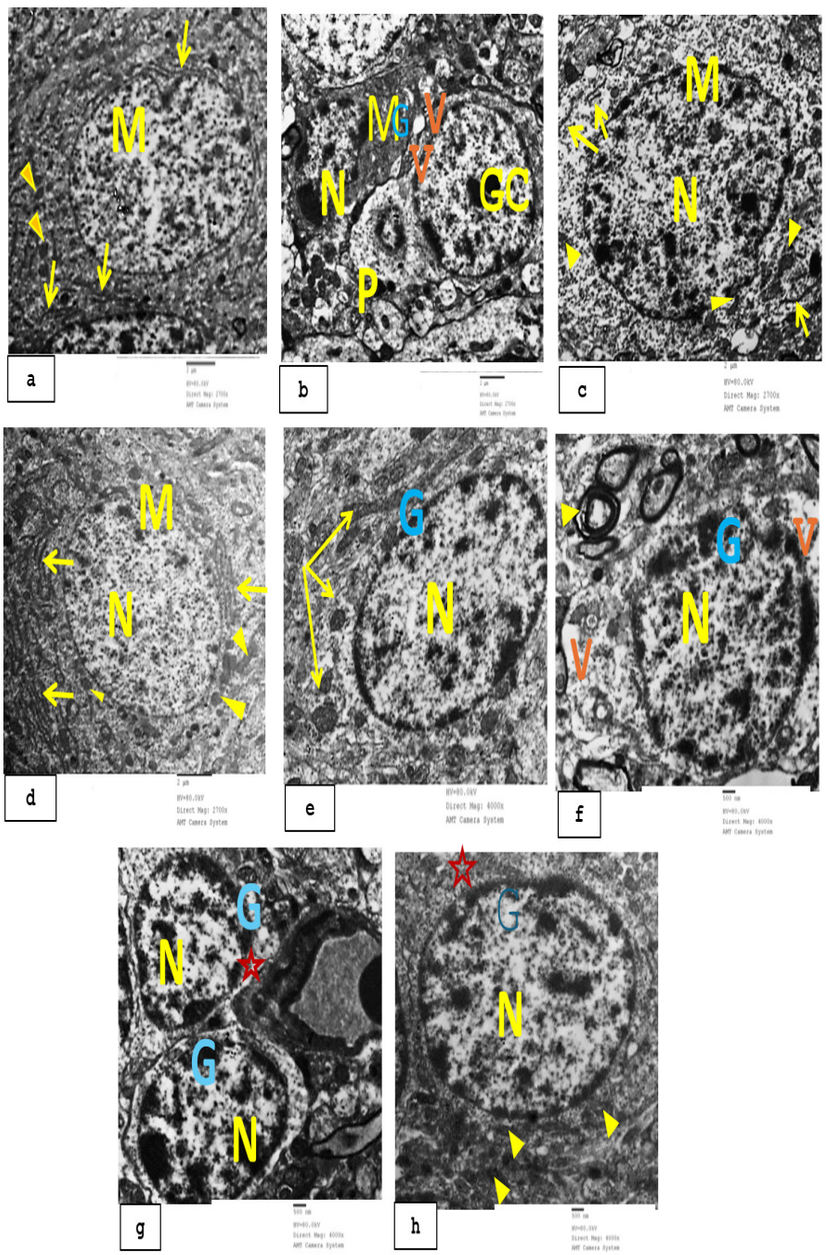

Figure 15: Electronmicrographs of the rat's olfactory bulb in diffirrent groups. a) Control group showing mitral cell (M) with central euchromatic nucleus and prominent nucleolus, well-defined abundant cytoplasm rich in rough endoplasmic reticulum (arrows) and mitochondria (arrow heads). b) ZnS group showing degenerating mitral nerve cell (M) with irregular nucleus (N) electron dense cytoplasm with vaculations (V) and dilated Golgi apparatus (G). Granule cell (GC) with its process (P) can be seen. c) ZnS+QU group showing a mitral nerve cell with euchromatic nucleus (N) and dispersed chromatin, r-ER (arrows) and mitochondria (arrow heads). d) ZnS+QU-CSNPs group treated group showing a mitral nerve cell (M) with euchromatic nucleus (N) and dispersed chromatin, r-ER (arrows) and mitochondria (arrow heads). e) Control group showing granule cell (G) with scanty cytoplasm and heterochromatic large nucleus (N). Notice apparently normal mitochondria (arrows). f) ZnS group showing a granule cell (G) with nucleus (N), vaculation of cytoplasm (V). Notice splitting of myelin sheath of an axon (arrow head). g) ZnS+QU group showing a granule cells (G) with large nuclei (N) and densily packed chromatin and surrounded by thin rim of cytoplasm (asterisks). h) ZnS+QU-CSNPs group showing granule cell (G) with large nucleus (N) and densily packed chromatin and surrounded by thin rim of cytoplasm (asterisk). Notice apparently normal mitochondria (arrow heads). (TEM: a, c, d X2700 e, f, g, h X4000).

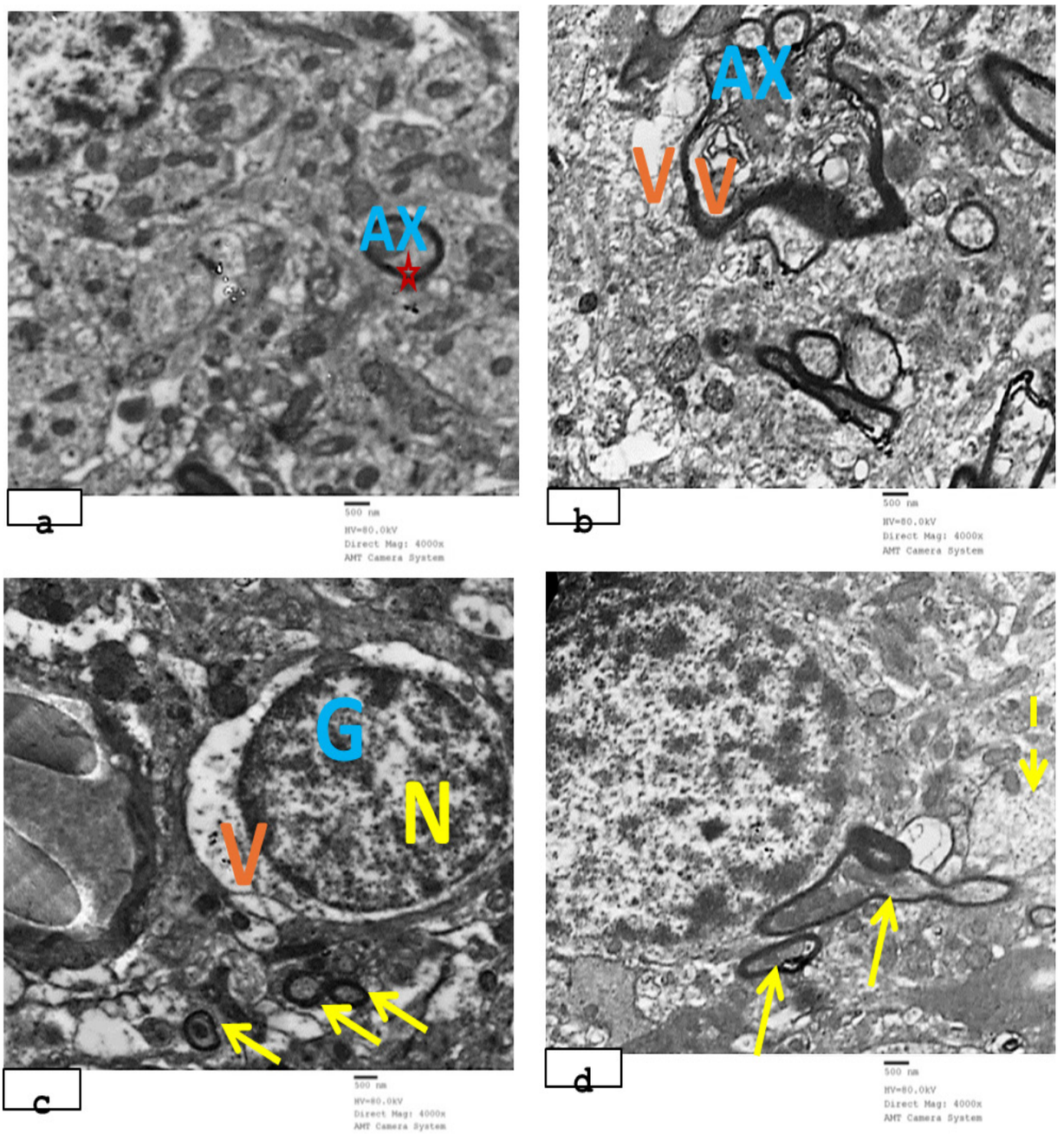

Figure 16: El Electronmicrographs of the rat's olfactory bulb in diffirrent groups showing: a) Control group showing axon (AX) with intact myelin sheath and compact myelin lamellae. Notice apparently normal mitochondria inside (asterisk). b) ZnS-group showing myelinated axon (AX) with irregular outline and axoplasm vaculation (V). Notice vaculation (V) in nueropil. c) ZnS+QU group showing intact myelinated axons (arrows).Notice granule cell (G) with large nucleus (N) and densily packed chromatin and vaculated cytoplasm (V). d) ZnS+QU-CSNPs group showing intact myelinated (arrows) and unmyelinated (dashed arrow) axons with mitochondria inside. (TEM: a, b, c, d X4000).

DISCUSSION

Olfactory dysfunctions are quite common disorders of the nose. Some of the causes of olfactory dysfunctions include nasal congestion, inflammation, infection, or injury to the olfactory epithelium, as well as anatomical and functional abnormalities of the olfactory nerve, olfactory bulb, or other components of the central nervous system[28]. Anosmia is the total absence of olfactory abilities, which impairs one's capacity to detect odors[9].

The loss of smell is considered an eminent, characteristic feature of SARS-CoV-2 associate disease (COVID-19). COVID-19 related olfactory dysfunction (hyposmia or anosmia) is very common (about 80 % of prevalence, depending on virus strains) and typically initial, short-term and transient. In most cases, olfaction returns within weeks from the infection. However, in 20 % of cases, patients can develop a persistent form of olfactory dysfunction (OD), which may last more than six months (or years) after the resolution of COVID-19[29].

Zinc sulfate (ZS) was used in numerous studies to induce anosmia by disrupting the olfactory epithelium[30]. Following tissue damage with ZnS, the olfactory epithelium's ability to degenerate appears to be variable. It indicates that multiple applications and the concentration applied enhance the efficiency of the treatment[31].

Several beneficial effects of quercetin have been identified, including antioxidant, anti-inflammatory, antibacterial, cardiovascular protection and cognitive impairment reversal[32]. But limitations like poor water solubility and low oral bioavailability render quercetin an insufficient candidate for therapeutic applications[33].

Several applications of nanoparticles as drug delivery systems, including the treatment of cancers, neurological diseases and cardiovascular diseases, have been well investigated[34]. Drug delivery systems, such as nanocarriers, are typically composed of lipids or polymers can enhance many of the pharmacologic characteristics of free medicines[35].

Because chitosan nanoparticles are biocompatible, bioactive, biodegradable and polycationic, they are commonly used as hydrophobic drug carriers to enhance their therapeutic efficacy and minimize their side effects[36].

This study aimed to investigate the potential prophylactic effect of QU and QU-CSNPs using ZnS as a model of anosmia and to evaluate whether administration of QU-CSNPs is more efficient than QU or have the same effect.

For physiological assessment, buried food test was performed to evaluate the olfactory function in all groups. In this study, ZnS group showed significant increase in the mean values of latency to find the cookie compared to other groups. This result could be attributed to loss of olfactory sensory neurons as reported by previous study following intranasal administration of ZnS. Regarding ZnS+QU-CSNPs treated group, there was a significant decrease in the mean values of latency to find the cookieif compared to ZnS+QU treated group[37]. Li *et al.*, 2021 studied the therapeutic effect of chitosan on an anosmic rat model and demonstrated that Chitosan may aid in the restoration of the olfactory function by regulating olfactory neuronal homeostasis in vivo[38].

Malondialdehyde (MDA) is widely used as a marker for oxidative stress and as an indicator of lipid peroxidation[39]. Free radicals cause lipid peroxidation, which damages lipid-rich regions like cell membranes or myelin sheaths and forms MDA[40]. Such membrane damage may ultimately result in cell death[41]. In the current study, MDA was measured in olfactory mucosa and bulb in all groups. This study showed that ZnS group showed significant increase in MDA level compared to other groups that was in line with previous work which studied the toxic effect of zinc oxide nanoparticles on rat cerebellum and revealed elevated MDA levels and decreased total antioxidants activity in cerebellum suggesting development of oxidative stress in zinc oxide nanoparticles treated group[42]. It was reported that ZnS and zinc oxide nanoparticles administration in common carp fish led to induction of oxidative stress and increased ROS (Reactive oxygen species)[43].

Regarding ZnS+QU-CSNPs treated group, there was significant decrease in MDA compared to Quercetin treated group. Similar result reported by previous work which studied the protective effect of QU and QU-CSNPs in doxorubicin induced cardiotoxicity and reported that QU showed a decrease in MDA levels, while QU-CSNPs showed a high pattern of decrease[36].

In addition to lowering lipid peroxidation, QU improves antioxidant enzyme activity and antioxidant levels to provide neuroprotection against oxidative stress[44]. TNF-α (Tumor Necrosis Factor-α) is one of the most significant pro-inflammatory cytokines, affecting various aspects of the immune reaction[45]. TNF-α directly affects physiologic function of olfactory neurons, independent of the

inflammatory cascade[46]. In the present work, TNF-α was measured as an inflammatory parameter in olfactory mucosa and bulb in all groups. This study showed that ZnS group showed significant increase in TNF-α levels compared to other groups, similar result was reported in olfactory bulb following administration of zinc oxide nanoparticles and demonstrated that oxidative stress induced release of pro -inflammatory cytokines including TNF –α[47]. As regard ZnS+QU-CSNPs treated group, there was a significant decrease in TNF-α levels compared to ZnS+QU treated group, similar result was reported by Hannan *et al*., 2023 in a rat model of arthritis and revealed decreased TNF-α levels in QU-CSNPs treated group[48]. Quercetin has anti-inflammatory properties through various mechanisms, one of which is the inhibition of pro-inflammatory cytokines production (TNF-α and IL-6) inhibiting cytokines, nitric oxide, production of prostaglandin and downregulating COX-2 expression[49].

Glutathione (GSH) is a tripeptide that acts as an endogenous antioxidant that affects many cellular functions[50] and is the most abundant antioxidant in cells[51]. In the current study, GSH was measured as an antioxidant parameter in olfactory mucosa and bulb in all groups. The present study showed that ZnS group showed significant decrease in GSH compared to other groups. This result can be explained as Zinc inhibits glutathione reductase and causes intracellular mitochondrial dysfunction, therefore interfering with GSH synthesis[52]. Regarding ZnS+QU-CSNPs treated group, there was significant increase in GSH compared to ZnS+QU treated group, similar result was shown by previous researchers[53]. This result could be attributed to the potential ability of quercetin to boost GSH levels and increase its antioxidant cellular capacity. When O2 - radicals are produced, GSH acts as a hydrogen donor in the processes that transform them into harmless H2O. Quercetin has been shown to enhance GSH levels, lower ROS and OH- radicals, which are mostly produced by mitochondria and restore redox balance[54].

In the current study, different structural changes were detected in the olfactory mucosa and olfactory bulb by light microscope in rats receiving intranasal irrigation with zinc sulfate.

H&E sections revealed that the olfactory mucosa and olfactory bulb from the control group displayed normal histological features. Regarding the olfactory mucosa following intranasal irrigation with ZnS, there was thinning of the olfactory epithelium with loss of its normal histological architecture, this was confirmed by morphometric analysis that showed that ZnS group had a significant decrease in olfactory epithelium thickness compared to other groups, the same findings were described by a previous work[55]. The basal cells were preserved as reported by Hsieh *et al.*, 2017 who studied the toxicity of intranasal instillation of Zinc gluconate on olfactory mucosa in mice[56]. Some areas in the lamina propria showed degeneration of Bowman's glands and nerve bundles as reported by previous study in their model of olfactory mucosa damage induced by olfactotoxin herbicide Dichlobenil and demonstrated that lamina propria appeared fibrotic and most of Bowman's glands and axon bundles had disappeared[57].

As for the olfactory bulb following intranasal irrigation with ZnS, there were thinning and loss of integrity of olfactory nerve layer (ONL) and distorted shape of glomeruli (GL), similar findings were reported by[58]. There were also, small darkly stained mitral cells with pyknotic nuclei with pericellular spaces and that was suggested before by other researchers who described these changes following exposure to formaldehyde[59].

The structural changes in olfactory mucosa and bulb could be attributed to the cytotoxic effects of zinc cation on several cell types such as neuronal PC12 cells[60], neurons and olfactory epithelium[56]. The mechanism causing zinc-mediated cell death appears to be oxidative necrosis[61].

Regarding olfactory mucosa of ZnS+QU treated group, there were areas showed replacement of olfactory epithelial cells with respiratory like columnar ciliated cells or respiratory metaplasia, similar findings were noticed previously after olfactory mucosa resection[62] and following exposure of rabbits to cigarette smoke[50]. Respiratory metaplasia could be explained as injury of olfactory epithelium could led to exhaustion of Globose basal cells and persistence of Horizontal basal cells which contribute to metaplastic respiratory epithelium[63].

Olfactory bulb of ZnS+QU treated group showed thinning and loss of integrity of olfactory nerve layer (ONL) and distorted shape of glomeruli (GL), while some mitral cells were apparently normal and others were darkly stained.

As regard olfactory mucosa and olfactory bulb of ZnS+QU-CSNPs treated group, QU-CSNPs had ameliorative effects on both olfactory mucosa and bulb and the histological architecture was preserved. These effects were consistent with other studies on different tissues as colon and brain[64].

According to what we have mentioned above, QU-CSNPs have better effects than QU as chitosan has the ability to bind to negatively charged body components including mucosal membranes, extending the period of contact and allowing any transported drug more time to penetrate. It is biodegradable and biocompatible[65], Moreover, high encapsulation efficiency, prolonged circulation time, controlled release and enhanced therapeutic efficacy are only a few of the powerful benefits that nanoparticles have over conventional delivery systems for hydrophobic drugs like QU. Quercetin has poor aqueous solubility, poor permeability, instability and poor bioavailability, in contrast[13] (Mukhopadhyay and Prajapati, 2015).

In the current study, Alcian blue-Periodic acid Schiff method was used for histochemical demonstration of polysaccharides contents of Bowman's glands, olfactory mucosa of ZnS group showed negative Alcian blue-Periodic acid Schiff reaction of Bowman's glands contents, similar finding was demonstrated by other investigators[62] in their models of olfactory mucosal damage. The result of the present work could be attributed to the cytotoxic effects of Zinc.

The olfactory mucosa of ZnS+QU and ZnS+QU-CSNPs treated groups showed positive Alcian blue-Periodic acid Schiff reaction of Bowman's glands contents and that could be attributed to the anti-inflammatory and antioxidant effects of quercetin[66] and hence preserve Bowman's glands.

As regards immunohistochemical study, SOX-2 is a marker of neural progenitor cells. Neural stem cells in the central nervous system produce the transcription factor Sox2 (SRY sex determining region Y-box 2), which is required for the pluripotency of embryonic stem cells. Sox2 is expressed in sustentacular cells, HBCs and a part of GBCs ORN (Olfactory receptors Neurons) progenitors) in the adult olfactory epithelium and is necessary for the transition from the activated state to a neuronal progenitor state[67].

In the current study, olfactory mucosa of ZnS group showed a significant decrease in the mean number of Sox2 immunopositive cells compared to ZnS+QU-CSNPs treated group, while showing no difference compared to ZnS+QU treated group which was confirmed by morphometric analysis, similar finding reported by[68] following exposure to cigarette smoke and observed that the number of SOX2+ ORN progenitors in the basal layer was approximately 20 % lower than in saline-treated mice on day 1 after final cigarette smoke administration. The olfactory mucosa of ZnS+QU-CSNPs treated group showed significant increase in the mean number of Sox2 immunopositive cells compared to ZnS+QU treated group and was confirmed by morphometric analysis, that was in line with[69] who reported that following Dasatinib and Quercetin treatment, there was an increased number of proliferating of SOX2+ PCNA+ non-glial progenitors (NGPs) in aged-injured killifish resulting in an increased generation of new mature neurons. The proliferating cell nuclear antigen (PCNA) was used in this study as a marker for cell proliferation.

Globose basal cells are identified by their position in the epithelium, by a high mitotic rate and by markers of cell division including Ki67, PCNA[70]. PCNA is a cell proliferation marker in the sub ventricular zone and olfactory bulb[71]. That was in line with a previous work[34] that reported there was low immunoreactivity of PCNA in olfactory mucosa in their model of anosmia. The olfactory bulb and rostral migratory stream of ZnS group showed significant decrease in the mean number of PCNA immunopositive cells compared to other groups and was confirmed by morphometric analysis. Previous studies have suggested that the olfactory function is associated with cell proliferation in the subventricular zone. In mice, olfactory dysfunction results from decreased subventricular zone cell proliferation, whereas olfactory function is improved following increased subventricular zone cell proliferation[72]. Excess zinc exacerbates the reduction of neurogenesis by affecting synaptic markers and rain-derived neurotrophic factor levels in the hippocampus and production of ROS[73]. The olfactory mucosa, olfactory bulb and rostral migratory stream of ZnS+QU-CSNPs treated group showed significant increase in the mean number of PCNA immunopositive cells compared to ZnS+QU treated group that was confirmed by morphometric analysis.

Quercetin nanoparticles administration retained proliferation through its activities as antioxidant, anti-inflammatory, pro-proliferative that promote DNA replication[74].

The mechanisms through which Quercetin enhanced proliferation and neurogenesis could also be explained according to[75] who reported that quercetin increased the number of cells that express doublecortin, which is expressed in dentate gyrus and the sub ventricular zone and increased the expression of neurotrophic factors as nerve growth

factor which control neurogenesis in rat model of Al Alzheimer's disease.

In the present study, COX-2 was used as a marker for inflammation. Eicosanoids are produced from arachidonic acid by the cyclooxygenase (COX) enzymes COX-1 and COX-2 and they are a crucial part and indicator of an inflammatory response[76].

In the current study, olfactory mucosa and olfactory bulb of ZnS group showed increase in the mean values of COX2 area fraction compared to other groups that was confirmed by morphometric analysis, similar findings were reported by[77] in olfactory mucosa following intranasal administration of lipopolysaccharide. This result could be explained that severe oxidative stress might activate Inflammation-related genes and transcription factors and thus would start the inflammatory process. COX-2 is induced in response to growth factors, cytokines and proinflammatory molecules[78].

The olfactory mucosa and olfactory bulb of ZnS+QU-CSNPs and ZnS+QU treated groups showed a significant decrease in the mean values of COX-2 area fraction compared to ZnS group confirmed by morphometric analysis, that was in line with[64] who reported that Quercetin loaded chitosan nanoparticles decreased the expression of COX-2 in a rat model of colitis.

The anti-inflammatory properties of flavonoids are explained by a variety of mechanisms. In the first mechanism, antioxidant and radical-scavenging activities are used. According to this mechanism, flavonoids considerably contribute to the anti-inflammatory activity of these substances by reducing the formation of active oxygen intermediates by neutrophils and other phagocytes[79]. Flavonoids efficiently inhibit the metabolism of arachidonic acid. It occurs as a result of the inhibition of gene expression of COX-1 (cyclooxygenase 1) and COX-2 (cyclooxygenase 2) enzymes[80].

For more survey, ultrastructure and components of cells by transmission electron microscope examination was done. Olfactory mucosa of ZnS group showed Bowman's gland with vacuolated cytoplasm, dilated r-ER cisternae and disrupted secretory granules, similar findings were reported by[81] in their models of anosmia.

Olfactory bulb of ZnS group showed degeneration of mitral cells with irregular nucleus, electron dense cytoplasm with vacuolation, irregular axons with splitting of myelin sheath and areas of vacuolated neuropil, these changes were described by[82] in cerebellum after intake of zinc oxide nanoparticles. Granule cells showed cytoplasmic vacuolation, similar finding reported by[83] following ozone exposure. The above structural alterations in the olfactory mucosa and bulb could be attributed to the cytotoxic and neurotoxic effects of Zn2+ Zn2+ is an effective inducer of ROS, which disrupts mitochondrial functions and causes cell necrosis or apoptosis[84].

Zinc accumulates within mitochondria[85] and excess Zn2+ stimulates the generation of mitochondrial ROS[86].

The axonal changes found in ZnS group could be explained as a result of a dying-back process of neuronal injury[87], increasing water content in degenerating nerves causes intramyelinic edema and edematous splitting at various levels of the myelin lamella, which is thought to be the cause of myelin sheath splitting[88]. As a sign of neuronal death, neuropil vacuolation may be caused by cells shrinking and withdrawing their processes as a result of cytoskeletal affection[87].

Acini of the Bowman's gland in the ZnS+QU treated group displayed dilated r-ER (rough endoplasmic reticulum) cisternae, which may be attributed to oxidative stress according to[89] who reported that oxidative stress alters the internal environment of the ER and results in persistent ER stress. When ROS attacks the ER, polyunsaturated fatty acids are peroxidized and a buildup of misfolded proteins forms in the ER lumen.

In the current study, Quercetin loaded chitosan nanoparticles had ameliorating effects on ultrastructure of both olfactory mucosa and bulb better than Quercetin, the neuroprotective effect of Quercetin nanoparticles was previously reported by[89] in rat model of Alzheimer's disease, also in a model of cerebral ischemia-induced injury, it has been demonstrated that a nano-encapsulated form of quercetin greatly reduces oxidative stress and improves neuronal protection in the hippocampus[90].

Quercetin is thought to be a potent antioxidant. It is a remarkable antioxidant and probably the best scavenger of reactive oxygen and nitrogen species because to its two antioxidant pharmacophores[91]. Quercetin could also be beneficial in the inhibition of oxidative stress-mediated neuronal damage as oxidative stress is considered as one of the major

causes of the development of neurodegenerative disorders and vascular pathologies in the brain due to its radical-scavenging and metal-chelating properties[92].

CONCLUSION

In conclusion, the previously mentioned data demonstrated that ZnS has damaging effects on olfactory mucosa and bulb. Inflammation and oxidative stress could be the mechanisms through which ZnS induces its damaging effects. The results indicated that QU-CSNPs have adequate prophylactic effects against damaging effects of ZnS and these effects were extremely superior to QU. These protective effects may be mediated by reducing oxidative stress, enhancing antioxidant defense mechanisms, controlling inflammation by lowering the levels of the pro-inflammatory cytokines TNF-α and improving the structural changes in olfactory mucosa and bulb. Additional studies are recommended to investigate further mechanisms underlying the potential beneficial effects of QU-CSNPs. Bring up a new line for anosmia therapy (it may be used as a potential therapy for anosmia caused by COVID-19). Additional clinical studies are needed to assess the safety, benefits and hazards of QU-CSNPs in humans..

CONFLICT OF INTEREST

There is no potential conflict of interest among the authors.

REFERENCES

1. Najafloo, R., *et al*., Mechanism of Anosmia Caused by Symptoms of COVID-19 and Emerging Treatments. ACS Chem Neurosci, 2021. 12(20): p. 3795 - 3805.

2. Topinkova, E., Smell and taste. Pathy's Principles and Practice of Geriatric Medicine, 2022. 2: p. 957 - 971.

3. Soler, Z.M., *et al*. A primer on viral-associated olfactory loss in the era of COVID-19. in International Forum of Allergy & Rhinology. 2020. Wiley Online Library.

4. Mutiawati, E., *et al*., Anosmia and dysgeusia in SARS-CoV-2 infection: incidence and effects on COVID-19 severity and mortality and the possible pathobiology mechanisms-a systematic review and meta-analysis. F1000Research, 2021. 10.

5. Doty, R.L., Clinical disorders of olfaction. Handbook of olfaction and gustation, 2015: p. 375 - 402.

6. Zhang, S.Q., *et al*., Comparison of the oral absorption, distribution, excretion and bioavailability of zinc sulfate, zinc gluconate and zinc-enriched yeast in rats. Molecular nutrition and food research, 2018. 62(7): p. 1700981.

7. Allan, G.M. and B. Arroll, Prevention and treatment of the common cold: making sense of the evidence. Cmaj, 2014. 186(3): p. 190 - 199.

8. Yokel, R.A., Direct nose to the brain nanomedicine delivery presents a formidable challenge. Wiley Interdisciplinary Reviews: Nanomedicine and Nanobiotechnology, 2022. 14(2): p. e1767.

9. Shahbaz, M.A., *et al.,* Mechanistic understanding of the olfactory neuroepithelium involvement leading to short-term anosmia in COVID-19 using the adverse outcome pathway framework. Cells, 2022. 11(19): p. 3027.

10. Azeem, M., *et al.,* An insight into anticancer, antioxidant, antimicrobial, antidiabetic and anti-inflammatory effects of quercetin: A review. Polymer Bulletin, 2023. 80(1): p. 241 - 262.

11. Shabir, I., *et al*., Promising bioactive properties of quercetin for potential food applications and health benefits: A review. Frontiers in nutrition, 2022. 9: p. 999752.

12. Sarfraz, M., *et al*., Resveratrol-laden nano-systems in the cancer environment: views and reviews. Cancers, 2023. 15(18): p. 4499.

13. Zang, X., *et al*., Quercetin nanoformulations: a promising strategy for tumor therapy. Food and function, 2021. 12(15): p. 6664 - 6681.

14. Imran, M., *et al*., The therapeutic and prophylactic potential of quercetin against COVID-19: An outlook on the clinical studies, inventive compositions and patent literature. Antioxidants, 2022. 11(5): p. 876.

15. Mitchell, M.J., *et al*., Engineering precision nanoparticles for drug delivery. Nature reviews drug discovery, 2021. 20(2): p. 101 - 124.

16. Pellis, A., G.M. Guebitz and G.S. Nyanhongo, Chitosan: Sources, processing and modification techniques. Gels, 2022. 8(7): p. 393.

17. Maghsoudnia, N., *et al*., Application of nano-based systems for drug delivery and targeting: a review. Journal of Nanoparticle Research, 2020. 22: p. 1 - 41.

18. Hasanin, M.T., *et al*., Production of well-dispersed aqueous cross-linked chitosan-based nanomaterials as alternative antimicrobial approach. Journal of Inorganic and Organometallic Polymers and Materials, 2018. 28: p. 1502 - 1510.

19. Ahn, S., *et al*., Transient anosmia induces depressive-like and anxiolytic-like behavior and reduces amygdalar corticotropin-releasing hormone in a ZnSO4-induced mouse model. Chemical senses, 2018. 43(4): p. 213 - 221.

20. Ågmo, A. and E.M. Snoeren, A cooperative function for multisensory stimuli in the induction of approach behavior of a potential mate. PLoS One, 2017. 12(3): p. e0174339.

21. Yang, M. and J.N. Crawley, Simple behavioral assessment of mouse olfaction. Current protocols in neuroscience, 2009. 48(1): p. 8.24. 112 .8.24-.

22. Baksi, R., *et al*., In vitro and in vivo anticancer efficacy potential of Quercetin loaded polymeric nanoparticles. Biomedicine & Pharmacotherapy, 2018. 106: p. 1513 - 1526.

23. Abdel Gawad, S., H. Ali and H. Fikry, Neuroregenerative role of transplanted olfactory ensheathing cells in a model of sciatic nerve crush injury in rats: Histological study. Egyptian Journal of Histology, 2017. 40(3): p. 362 - 373.

24. Bahaa, N. and M. Raafat, Effect of intranasally-administered adipose derived stem cells on age-related changes of rat olfactory bulb: A histological and immunohistochemical study. Egyptian Journal of Histology, 2017. 40(4): p. 459 - 475.

25. Amer, A.S. and D.A. Zaghloul, Effects of Nicotine and Its Withdrawal on The Postnatal Development of Rat Mitral Cells. Egyptian Academic Journal of Biological Sciences, D. Histology & Histochemistry, 2021. 13(2): p. 135 - 150.

26. Suvarna, K.S., C. Layton and J.D. Bancroft, Bancroft's theory and practice of histological techniques E-Book. 2018: Elsevier health sciences.

27. Côté, S., Current protocol for light microscopy immunocytochemistry. Immunohistochemistry, II, 1993: p. 148 - 167.

28. Liang, F. and D.Y. Wang, COVID-19 anosmia: high prevalence, plural neuropathogenic mechanisms and scarce neurotropism of SARS-CoV-2? Viruses, 2021. 13(11): p. 2225.

29. Lechien, J.R., L.A. Vaira and S. Saussez, Prevalence and 24-month recovery of olfactory dysfunction in COVID-19 patients: A multicentre prospective study. Journal of internal medicine, 2023. 293(1): p. 82 - 90.

30. Takahashi, K., *et al*., Donepezil prevents olfactory dysfunction and α-synuclein aggregation in the olfactory bulb by enhancing autophagy in zinc sulfate-treated mice. Behavioural Brain Research, 2023. 438: p. 114175.

31. Ahn, S., *et al*., Chronic anosmia induces depressive behavior and reduced anxiety via dysregulation of glucocorticoid receptor and corticotropin-releasing hormone in a mouse model. Rhinology, 2016. 54(1): p. 80 - 87.

32. Lawson, M.K., Improvement of therapeutic value of quercetin with chitosan nanoparticle delivery systems and potential applications. International Journal of Molecular Sciences, 2023. 24(4): p. 3293.

33. Tomou, E.-M., *et al.,* Recent advances in nanoformulations for quercetin delivery. Pharmaceutics, 2023. 15(6): p. 1656.

34. Yoo, S.H., H.-W. Kim and J.H. Lee, Restoration of olfactory dysfunctions by nanomaterials and stem cells-based therapies: Current status and future perspectives. Journal of Tissue Engineering, 2022. 13: p. 20417314221083414.

35. Sangnim, T., *et al.,* Chitosan in oral drug delivery formulations: A review. Pharmaceutics, 2023. 15(9): p. 2361.

36. Soliman, A.G., *et al.*, Optimized synthesis characterization and protective activity of quercetin and quercetin–chitosan nanoformula against cardiotoxicity that was induced in male Wister rats via anticancer agent: Doxorubicin. Cancer Nanotechnology, 2023. 14(1): p. 10.

37. Cho, H.-J., *et al*., Newly developed method for mouse olfactory behavior tests using an automatic

video tracking system. Auris Nasus Larynx, 2018. 45(1): p. 103110-.

38. Li, S.-T., T.-H. Young and T.-W. Huang, Regeneration of olfactory neuroepithelium in 3-methylindole-induced anosmic rats treated with intranasal chitosan. Biomaterials, 2021. 271: p. 120738.

39. Zanjani, B.N., *et al*., Plasma levels of oxysterols 7-ketocholesterol and cholestane-3β, 5α, 6β-triol in patients with allergic asthma. Journal of Asthma, 2022: p. 110-.

40. Ghonimi, N.A., *et al*., Serum malondialdehyde as a lipid peroxidation marker in multiple sclerosis patients and its relation to disease characteristics. Multiple sclerosis and related disorders, 2021. 51: p. 102941.

41. Nazarizadeh, A. and S. Asri-Rezaie, Comparative study of antidiabetic activity and oxidative stress induced by zinc oxide nanoparticles and zinc sulfate in diabetic rats. AAPS PharmSciTech, 2016. 17: p. 834843-.

42. Amer, M.G. and R.A. Karam, Morphological and biochemical features of cerebellar cortex after exposure to zinc oxide nanoparticles: possible protective role of curcumin. The Anatomical Record, 2018. 301(8): p. 14541466-.

43. Deepa, S., *et al*., Effects of zinc oxide nanoparticles and zinc sulfate on the testis of common carp, Cyprinus carpio. Nanotoxicology, 2019. 13(2): p. 240257-.

44. Kumar, A., *et al*., Deltamethrin-induced immunotoxicity and its protection by quercetin: an experimental study. Endocrine, Metabolic & Immune Disorders-Drug Targets (Formerly Current Drug Targets-Immune, Endocrine & Metabolic Disorders), 2020. 20(1): p. 6776-.

45. Filik, H. and A.A. Avan, Electrochemical immunosensors for the detection of cytokine tumor necrosis factor alpha: a review. Talanta, 2020. 211: p. 120758.

46. Sultan, B., L.A. May and A.P. Lane, The role of TNF-α in inflammatory olfactory loss. The Laryngoscope, 2011. 121(11): p. 24812486-.

47. Wei, S., *et al*., Chemosensory dysfunction induced by environmental pollutants and its potential as a novel neurotoxicological indicator: a review. Environmental science & technology, 2021. 55(16): p. 1091110922-.

48. Hannan, A., *et al*., Quercetin-loaded chitosan nanoparticles ameliorate adjuvant-induced arthritis in rats by regulating anti-oxidant enzymes and downregulating pro-and inflammatory cytokines. Inflammopharmacology, 2023. 31(1): p. 287300-.

49. Wei, E., *et al*., Ginsenoside Rb1 alleviates lipopolysaccharide-induced inflammatory injury by downregulating miR-222 in WI-38 cells. Cell transplantation, 2021. 30: p. 09636897211002787.

50. Iskusnykh, I.Y., A.A. Zakharova and D. Pathak, Glutathione in brain disorders and aging. Molecules, 2022. 27(1): p. 324.

51. Matuz-Mares, D., *et al*., Glutathione participation in the prevention of cardiovascular diseases. Antioxidants, 2021. 10(8): p. 1220.

52. Choi, S., *et al*., Zinc in the brain: friend or foe? International Journal of Molecular Sciences, 2020. 21(23): p. 8941.

53. AbdElrazek, D.A., *et al*., Neuroprotective effect of quercetin and nano-quercetin against cyclophosphamide-induced oxidative stress in the rat brain: Role of Nrf2/HO-1/Keap-1 signaling pathway. Neurotoxicology, 2023. 98: p. 1628-.

54. Akyuz, E., *et al*., Enlightening the neuroprotective effect of quercetin in epilepsy: From mechanism to therapeutic opportunities. Epilepsy & Behavior, 2021. 115: p. 107701.

55. Chalansonnet, M., *et al*., Study of potential transfer of aluminum to the brain via the olfactory pathway. Toxicology Letters, 2018. 283: p. 7785-.

56. Hsieh, H., M.C. Horwath and M.B. Genter, Zinc gluconate toxicity in wild-type vs. MT12-/deficient mice. Neurotoxicology, 2017. 58: p. 130136-.

57. Franceschini, V., *et al*., Transplanted human adipose tissue-derived stem cells engraft and induce regeneration in mice olfactory neuroepithelium in response to dichlobenil subministration. Chemical Senses, 2014. 39(7): p. 617629-.

58. LaFever, B.J. and F. Imamura, Effects of nasal inflammation on the olfactory bulb. Journal of neuroinflammation, 2022. 19(1): p. 294.

59. Elsaid, A. and N.M. Faheem, Ameliorative effects of Omega-3 on the formaldehyde-induced damage in rat olfactory bulb. Egyptian Journal of Histology, 2023. 46(1): p. 7890-.

60. Kao, Y.-Y., *et al*., Demonstration of an olfactory bulb–brain translocation pathway for ZnO nanoparticles in rodent cells in vitro and in vivo. Journal of Molecular Neuroscience, 2012. 48: p. 464471-.

61. Krzywoszyńska, K., *et al*., General aspects of metal ions as signaling agents in health and disease. Biomolecules, 2020. 10(10): p. 1417.

62. Mori, E., *et al*., Squamous and respiratory metaplasia after olfactory mucosal resection. Frontiers in Neuroscience, 2021. 15: p. 695653.

63. Kay, L.M., COVID-19 and olfactory dysfunction: a looming wave of dementia? Journal of Neurophysiology, 2022. 128(2): p. 436444-.

64. Khater, S.I., *et al*., Therapeutic potential of quercetin loaded nanoparticles: Novel insights in alleviating colitis in an experimental DSS induced colitis model. Biomedicines, 2022. 10(7): p. 1654.

65. Bandi, S.P., S. Bhatnagar and V.V.K. Venuganti, Advanced materials for drug delivery across mucosal barriers. Acta biomaterialia, 2021. 119: p. 1329-.

66. Tang, J., *et al*., Quercetin and quercitrin attenuates the inflammatory response and oxidative stress in LPS-induced RAW264. 7 cells: in vitro assessment and a theoretical model. BioMed research international, 2019. 2019.

67. Guo, Z., Maintenance, differentiation and regulation of multipotent progenitor cells in the olfactory epithelium. 2008, Tufts University-Graduate School of Biomedical Sciences.

68. Ueha, R., *et al*., Damage to Olfactory Progenitor Cells Is Involved in Cigarette Smoke–Induced Olfactory Dysfunction in Mice. The American journal of pathology, 2016. 186(3): p. 579586-.

69. Van Houcke, J., *et al*., A short dasatinib and quercetin treatment is sufficient to reinstate potent adult neuroregenesis in the aged killifish. npj Regenerative Medicine, 2023. 8(1): p. 31.

70. Finger, T.E., *et al*., 5HTR3A-driven GFP labels immature olfactory sensory neurons. Journal of Comparative Neurology, 2017. 525(7): p. 1743-1755.

71. Ogawa, B., *et al*., Repeated administration of acrylamide for 28 days suppresses adult neurogenesis of the olfactory bulb in young-adult rats. Toxicology Letters, 2023. 378: p. 19-.

72. Marin, C., *et al*., Olfactory dysfunction in traumatic brain injury: the role of neurogenesis. Current Allergy and Asthma Reports, 2020. 20: p. 111-.

73. Nam, S.M., *et al*., Differential effects of low- and high-dose zinc supplementation on synaptic plasticity and neurogenesis in the hippocampus of control and high-fat diet-fed mice. Neurochemical Research, 2017. 42: p. 31493159-.

74. Kong, Y., *et al*., Quercetin ameliorates Aβ toxicity in Drosophila AD model by modulating cell cycle-related protein expression. Oncotarget, 2016. 7(42): p. 67716.

75. Karimipour, M., *et al*., Quercetin promotes learning and memory performance concomitantly with neural stem/progenitor cell proliferation and neurogenesis in the adult rat dentate gyrus. International Journal of Developmental Neuroscience, 2019. 74: p. 18-26.

76. Sagit, M., *et al*., Effectiveness of quercetin in an experimental rat model of allergic rhinitis. European Archives of Oto-Rhino-Laryngology, 2017. 274: p. 30873095-.

77. Tiboc-Schnell, C., *et al*., Quercetin attenuates naso-sinusal inflammation and inflammatory response in lungs and brain on an experimental model of acute rhinosinusitis in rats. Journal of Physiology & Pharmacology, 2020. 71(4).

78. Nasry, W.H.S., J.C. Rodriguez-Lecompte and C.K. Martin, Role of COX-2/PGE2 mediated inflammation in oral squamous cell carcinoma. Cancers, 2018. 10(10): p. 348.

79. Saini, N., S. Gahlawat and V. Lather, Flavonoids: A nutraceutical and its role as anti-inflammatory and anticancer agent. Plant biotechnology: Recent advancements and developments, 2017: p. 255 - 270.

80. Raja, S., I. Ramya and K. Ravindranadh, A review on protective role of phytoconstituents against isoproterenol induced myocardial

necrosis. Int J Pharmacogn Phytochem Res, 2016. 8(5): p. 848 - 864.

81. Franzén, A., *et al*., CYP2A5-mediated activation and early ultrastructural changes in the olfactory mucosa: studies on 2, 6-dichlorophenyl methylsulfone. Drug metabolism and disposition, 2006. 34(1): p. 61 - 68.

82. Abdel-aziz, H., N.H. Mekawy and N.E. Ibrahem, Histological and immunohistochemical study on the effect of zinc oxide nanoparticles on cerebellar cortex of adult male albino rats. Egyptian Journal of Histology, 2019. 42(1): p. 23 - 34.

83. BARENQUE, L.C.N., *et al*., Morphological recovery of the granule cells from the olfactory bulb after the cessation of acute ozone exposure. International journal of neuroscience, 2005. 115(3): p. 411 - 421.

84. Skrajnowska, D. and B. Bobrowska-Korczak, Role of zinc in immune system and anti-cancer defense mechanisms. Nutrients, 2019. 11(10): p. 2273.

85. Qi, Z., *et al*., Zinc accumulation in mitochondria promotes ischemia-induced BBB disruption through Drp1-dependent mitochondria fission. Toxicology and Applied Pharmacology, 2019. 377: p. 114601.

86. Lee, S.R., Critical role of zinc as either an antioxidant or a prooxidant in cellular systems. Oxidative medicine and cellular longevity, 2018. 2018.

87. Afifi, O.K. and A.S. Embaby, Histological study on the protective role of ascorbic acid on cadmium induced cerebral cortical neurotoxicity in adult male albino rats. Journal of microscopy and ultrastructure, 2016. 4(1): p. 36 - 45.

88. Weil, M.-T., *et al*., Loss of myelin basic protein function triggers myelin breakdown in models of demyelinating diseases. Cell reports, 2016. 16(2): p. 314 - 322.

89. Shao, B., *et al*., Protective effect of caffeic acid phenethyl ester against imidacloprid-induced hepatotoxicity by attenuating oxidative stress, endoplasmic reticulum stress, inflammation and apoptosis. Pesticide biochemistry and physiology, 2020. 164: p. 122 - 129.

90. Ghosh, A., *et al*., Neuroprotective role of nanoencapsulated quercetin in combating ischemia-reperfusion induced neuronal damage in young and aged rats. PloS one, 2013. 8(4): p. e57735.

91. Salehi, B., *et al*., Therapeutic potential of quercetin: new insights and perspectives for human health. ACS omega, 2020. 5(20): p. 11849 - 11872.

92. Suganthy, N., *et al*., Bioactive effects of quercetin in the central nervous system: Focusing on the mechanisms of actions. Biomedicine & Pharmacotherapy, 2016. 84: p. 892 - 908.

الملخص العربي

التأثيرات الوقائية المحتملة للكيرسيتين مقابل حبيبات الكيتوزان النانوية المحملة بالكيرسيتين على إصابة الغشاء المخاطي الشمي والبصلة الناتج عن كبريتات الزنك في ذكور الجرذان البيضاء البالغة؛ دراسة سلوكية بيوكيميائية وهستولوجية وهستوكيميائية مناعية

علياء حمدي عبد الحليم[1]، أميرة فتحي أحمد[1]، راندا أحمد ابراهيم[1]، سيد فؤاد الشيخ[2]،
ولاء يحيي عبد الظاهر[3]، عزة حسين علي[1]، سارة محمد نجيب عبد الحافظ[1]
[1]قسم الهستولوجيا وبيولوجيا الخلية - [2]قسم التشريح وعلم الأجنة - [3]قسم الفارماكولوجي
الطبية - كلية الطب - جامعة المنيا - المنيا - جمهورية مصر العربية

الخلفية: فقدان الشم هو مشكلة مزعجة شائعة تؤثر على نوعية الحياة. تعمل الجسيمات النانوية كحاملات نانوية تقوم بتوصيل حمولات دوائية قوية بمعدل متحكم فيه في الموقع المستهدف.

الهدف من البحث: يهدف هذا العمل الحالي إلى تقييم الفوائد الوقائية المحتملة للكيرسيتين مقابل حبيبات الكيتوزان النانوية المحملة بالكيرسيتين على نموذج فأر تجريبي لفقد الشم وإلقاء نظرة ثاقبة على آليات الحماية الخاصة به.

طريقة البحث: تم تقسيم أربعين فأراً عشوائياً إلى أربع مجموعات، المجموعة الضابطة، مجموعة كبريتات الزنك، مجموعة كبريتات الزنك+الكيرسيتين، ومجموعة كبريتات الزنك+حبيبات الكيتوزان النانوية المحملة بالكيرسيتين. تم إجراء التقييم السلوكي. تم جمع الغشاء المخاطي الشمي والبصلة للتحليل الكيميائي الحيوي والنسيجي والكيميائي المناعي والمورفومتري.

نتائج البحث: أظهرت مجموعة كبريتات الزنك تغيرا سلوكيًا، وانخفاض مستويات GSH، وزيادة مستويات MDA، وTNF-α. أظهر الغشاء المخاطي الشمي والبصلة تغيرات نسيجية، بالإضافة إلى زيادة كبيرة في التعبير المناعي لـ COX-2 وانخفاض في التعبير المناعي ل PCNA وSOX2. أظهرت مجموعة كبريتات الزنك+ حبيبات الكيتوزان النانوية المحملة بالكيرسيتين تحسنًا في المؤشرات المذكورة مسبقًا والتغير النسيجي مقارنة بمجموعة كبريتات الزنك+الكيرسيتين.

الاستنتاجات: حبيبات الكيتوزان النانوية المحملة بالكيرسيتين لها تأثيرات وقائية في نموذج فقدان الشم مقارنة بالكيرسيتين عبر آثاره المضادة للالتهابات والمضادة للأكسدة. وهذا يمكن أن يمهد الطريق لإجراء دراسات إضافية لاستكشاف المزيد من الآليات الكامنة وراء التأثيرات المفيدة المحتملة لحبيبات الكيتوزان النانوية المحملة بالكيرسيتين وطرح خط جديد لعلاج فقدان الشم.